# Designing Oxide Catalysts for Oxygen Electrocatalysis: Insights from Mechanism to Application

Ning Han[1], Wei Zhang[1], Wei Guo[1], Hui Pan[3], Bo Jiang[4], Lingbao Xing[5] ✉, Hao Tian[6] ✉, Guoxiu Wang[6], Xuan Zhang[1,2] ✉, Jan Fransaer[1] ✉

HIGHLIGHTS

- Fundamental principles underlying the design of oxide catalysts, including the influence of crystal structure, and electronic structure on their performance are summarized and analyzed.

- Challenges associated with developing oxide catalysts and the potential strategies are discussed.

ABSTRACT The electrochemical oxygen reduction reaction (ORR) and oxygen evolution reaction (OER) are fundamental processes in a range of energy conversion devices such as fuel cells and metal–air batteries. ORR and OER both have significant activation barriers, which severely limit the overall performance of energy conversion devices that utilize ORR/OER. Meanwhile, ORR is another very important electrochemical reaction involving oxygen that has been widely investigated. ORR occurs in aqueous solutions via two pathways: the direct 4-electron reduction or 2-electron reduction pathways from O_2 to water (H_2O) or from O_2 to hydrogen peroxide (H_2O_2). Noble metal electrocatalysts are often used to catalyze OER and ORR, despite the fact that noble metal electrocatalysts have certain intrinsic limitations, such as low storage. Thus, it is urgent to develop more active and stable low-cost electrocatalysts, especially for severe environments (e.g., acidic media). Theoretically, an ideal oxygen electrocatalyst should provide adequate binding to oxygen species. Transition metals not

belonging to the platinum group metal-based oxides are a low-cost substance that could give a d orbital for oxygen species binding. As a result, transition metal oxides are regarded as a substitute for typical precious metal oxygen electrocatalysts. However, the development of oxide catalysts for oxygen reduction and oxygen evolution reactions still faces significant challenges, e.g., catalytic activity, stability, cost, and reaction mechanism. We discuss the fundamental principles underlying the design of oxide catalysts, including the influence of
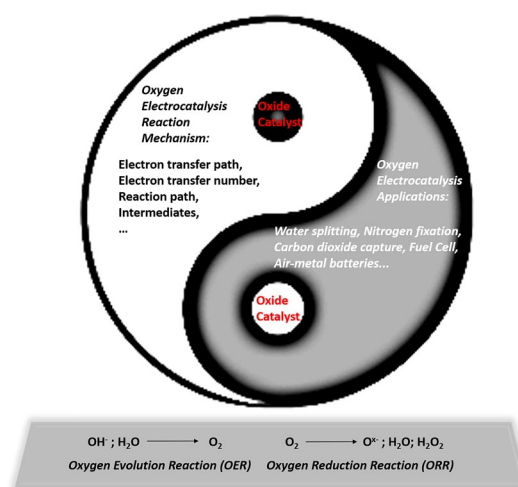
✉ Lingbao Xing, lbxing@sdut.edu.cn; Hao Tian, hao.tian@uts.edu.au; Xuan Zhang, xuanzhangzju@zju.edu.cn; Jan Fransaer, jan.fransaer@kuleuven.be

1. Department of Materials Engineering, KU Leuven, 3001 Leuven, Belgium
2. ZJU-Hangzhou Global Scientific and Technological Innovation Centre, Zhejiang University, Hangzhou 311200, People's Republic of China
3. Department of Physics and Astronomy, KU Leuven, 3001 Leuven, Belgium
4. Key Laboratory of Ocean Energy Utilization and Energy Conservation of Ministry of Education, Dalian University of Technology, Dalian 116023, People's Republic of China
5. School of Chemistry and Chemical Engineering, Shandong University of Technology, Zibo 255000, People's Republic of China
6. Centre for Clean Energy Technology, Faculty of Science, University of Technology Sydney, Broadway, PO Box 123, Ultimo, NSW 2007, Australia

crystal structure, and electronic structure on their performance. We also discuss the challenges associated with developing oxide catalysts and the potential strategies to overcome these challenges.

1 Problem Statement

The growing energy demand caused by population increase has resulted in the accelerated use of fossil fuels and serious environmental consequences [1–5]. The depletion of fossil fuel reserves, combined with the urgent need to reduce greenhouse gas emissions in order to combat climate change, has inexorably pushed humans to transform the existing electricity generating grid into more renewable and sustainable alternative structures [6–10]. The difficulty in using renewable energy (such as solar, wind, and hydropower) is that it is intermittent, necessitating the development of energy storage and conversion technologies to deliver energy when it is needed [11–13]. Because of its high mass-energy density and absence of greenhouse gas emissions, hydrogen is a potential alternative energy carrier for replacing the existing fossil fuel grid [14–16]. The bulk of hydrogen generation is hampered by the costly and energy-intensive steam reforming of hydrocarbons, which are mostly derived from fossil fuels and emit large amounts of pollutants [17–20]. Cost-effective hydrogen production technologies are required for the adoption of renewable energy projects [17, 21–23]. Despite the technological challenges, electrochemical water splitting is a promising method of producing hydrogen-28]. Electricity may be stored in the chemical bond of H_2 through electrochemical splitting of water, and electricity can be generated later by recombining H_2 with O_2 in a fuel cell [24–27]. In this respect, it is worth noting that the most prevalent element in the Earth's crust is oxygen [28–34]. Oxygen reduction is also the most essential reaction in life processes (e.g., biological respiration) and energy conversion devices (e.g., fuel cells). Water electrolysis and fuel cell technology with a high efficiency are needed to realize this plan. Because the oxygen evolution reaction (OER) at the anode is kinetically much slower than the hydrogen evolution reaction (HER) at the cathode, it dominates the efficiency of water electrolysis [35–37]. For fuel cells, the oxygen reduction reaction (ORR) is the slowest half-reaction mainly relying on rare noble metal catalysts [38–44]. Thus, it is important to conduct investigations on oxygen electrodes (OER and ORR).

Oxygen (O_2) electrochemistry is the study of the electrocatalysis or reduction of molecular oxygen [45]. The oxygen evolution reaction (OER) is the generation of O_2 molecules by removing electrons from water reactant, whereas O_2 molecules combine with electrons to produce through oxygen reduction reaction (ORR). Because of its complexity and relevance in many practical technologies and industrial processes, oxygen electrocatalysis has been extensively explored. It is particularly important in numerous renewable energy technologies, including water electrolysis, fuel cells, and other industrial uses. Before catalyst design, it is necessary to understand the reaction path and reaction mechanism. Briefly speaking, OER is the electrochemical reaction that produces oxygen molecules via a series of coupled proton/electron steps. The reaction pathways are quite different in acidic and alkaline electrolytes [46, 47]. Hydroxyl groups (OH^-) are oxidized in alkaline electrolytes and transformed into water (H_2O) and oxygen molecules (O_2) [48], while two water molecules (H_2O) are oxidized in acidic electrolytes to produce four protons (H^+) and one oxygen molecule (O_2) [11, 49]. Due to the abundance of hydroxyl groups in the electrolyte, alkaline OER has more favorable reaction kinetics than acidic OER [50, 51]. For acidic OER, a high energy is needed to break the strong covalent O–H bond in H_2O, which results in slow kinetics and worse OER performance [25, 52–54]. In spite of more favorable kinetics for alkaline OER, acidic OER is more applicable to commercialization because of the successful development and large-scale applications of proton exchange membrane (PEM) [55]. Thus, the promising electrocatalysts for OER should be not only active for oxygen thermodynamic reaction but also conquer the kinetic barriers. Meanwhile, ORR, another very important oxygen electrocatalysis, has been widely investigated. ORR in aqueous solutions is mostly accomplished through two pathways: the direct 4-electron reduction or 2-electron reduction from O_2 to water (H_2O) or hydrogen peroxide (H_2O_2), respectively [56, 57]. There are multiple different reaction routes depending on the pH of the electrolyte and catalyst. The dissociative and associative routes are two putative response pathways for the ORR mechanism. The O–O bond is disrupted as O_2 is adsorbed onto two metal

active sites through the dissociative pathway. As a result, no peroxide intermediate is produced. The O–O bond in oxygen molecules is difficult to break, making the dissociative pathway unlikely for most catalysts. For the associative route, the O_2 is adsorbed onto a single metal site, which makes it easier to break the O–O bond and give rise to the formation of a peroxide intermediate. Evaluating the OER and ORR reaction processes can lead to the design of the optimal catalyst by identifying the catalyst characteristics for maximal electrocatalysis activity and selecting the target chemicals [45, 58–60].

An excellent oxygen electrocatalyst should provide adequate binding to oxygen species (neither too strong nor too weak). Until now, noble metal-based materials such as Ir, Ru, and Pt have shown to be the ideal catalysts for the oxygen electrocatalysis [61–64]. The high cost and scarcity of these precious metals limit their widespread use. From the standpoint of commercialization, it is not just the high cost of noble metal components that causes economic strain, but also the increased costs incurred due to the difficulties of manufacturing multiple cathode–anode products and potential cross-contaminations [65, 66]. As a result, a lot of effort has gone into developing efficient and low-cost oxygen electrocatalysts for OER/ORR [67, 68]. Transition metal oxides not belonging to the platinum group metals are a low-cost material type providing a d orbital for the binding of oxygen species. Among the transition metal oxide catalysts, the perovskite-like catalysts, such as single perovskites (ABO_3) [69–71], double perovskites ($A_2B_2O_6$) [72, 73], Ruddlesden–Popper perovskites (A_2BO_4) [74–76], and pyrochlore-type oxides ($A_2B_2O_7$) [77], have gained recognition as materials for electrochemical catalysts due to the low cost of transition metals in the crystal [78], robust skeletal structure, intrinsic nature of harboring oxygen vacancies, electronic structural versatility, and compositional flexibility [25]. Perovskite-like oxides can work as oxygen conductors, proton conductors, or mixed ionic-electronic conductors depending on the occupancy of various metal ions in the A and B sites; thus, it has been employed as functional materials in energy and environmental domains during the last few decades [79–85]. To create effective perovskite-like electrocatalysts, researchers should focus more on the fundamental principles of developing perovskite materials and the relationship between catalysts and reaction processes [86–90]. Because electrocatalytic reactions generally entail the transfer of electrons, oxide catalysts with high electronic and ionic conductivity likely have superior electrocatalytic performance [90, 91]. The high electrical conductivity of catalysts reduces the ohmic losses and enhances the catalytic efficiencies in electrochemical devices. Based on the fundamental understanding of reaction paths, research has been performed on the development of various highly active, low-cost perovskite-like oxide catalysts for oxygen electrocatalysis and related applications [86, 92–94].

2 General Principles of Oxygen Electrolysis

2.1 Reaction Mechanism of Oxygen Evolution

The OER is a complex reaction that involves the transfer of four electrons [69, 95]. The conventional adsorbate evolution-dominated mechanism (AEM) proceeds via a sequence of concerted electron–proton transfers on the transition metal active centers, and binding of the adsorbed oxygen intermediates should be neither too strong nor too weak, leading to (ΔG_{O*}-ΔG_{HO*}) of 1.6 eV, according to the Sabatier's principle [78, 96]. According to the AEM mechanism, the intermediate M–OH is initially formed by a one-electron oxidation of hydroxide anion on the basis of surface metal sites (M) as a catalytically active site. Then, the M–OH is converted to M–O via the electron transfer and proton coupling step. When a hydroxide anion undergoes one-electron oxidation, M–O converts to M–OOH, which then undergoes another electron transfer and proton coupling process to produce O_2 molecules. In contrast to the OER process in alkaline media, the initial step in the acidic media is the adsorption of H_2O on M (Fig. 1a), followed by the water dissociation to form M-OH and second proton release to form M–O. Following that, another water molecule nucleophilically attacks M–O, culminating in the generation of M–OOH.

In recent years, a novel mechanism based on the redox chemistry of lattice oxygen anions, known as the lattice oxygen-mediated mechanism (LOM), which differs from the well-known AEM, has been proposed. This mechanism is validated by ^{18}O isotope detection of the reaction product as well as density functional theory calculations and entails the direct participation of oxygen anions from the oxide catalysts lattice as an active intermediate in the OER [89, 97–100]. LOM can bypass the scaling limitations of the conventional AEM and lead to better OER kinetics. For example, LOM
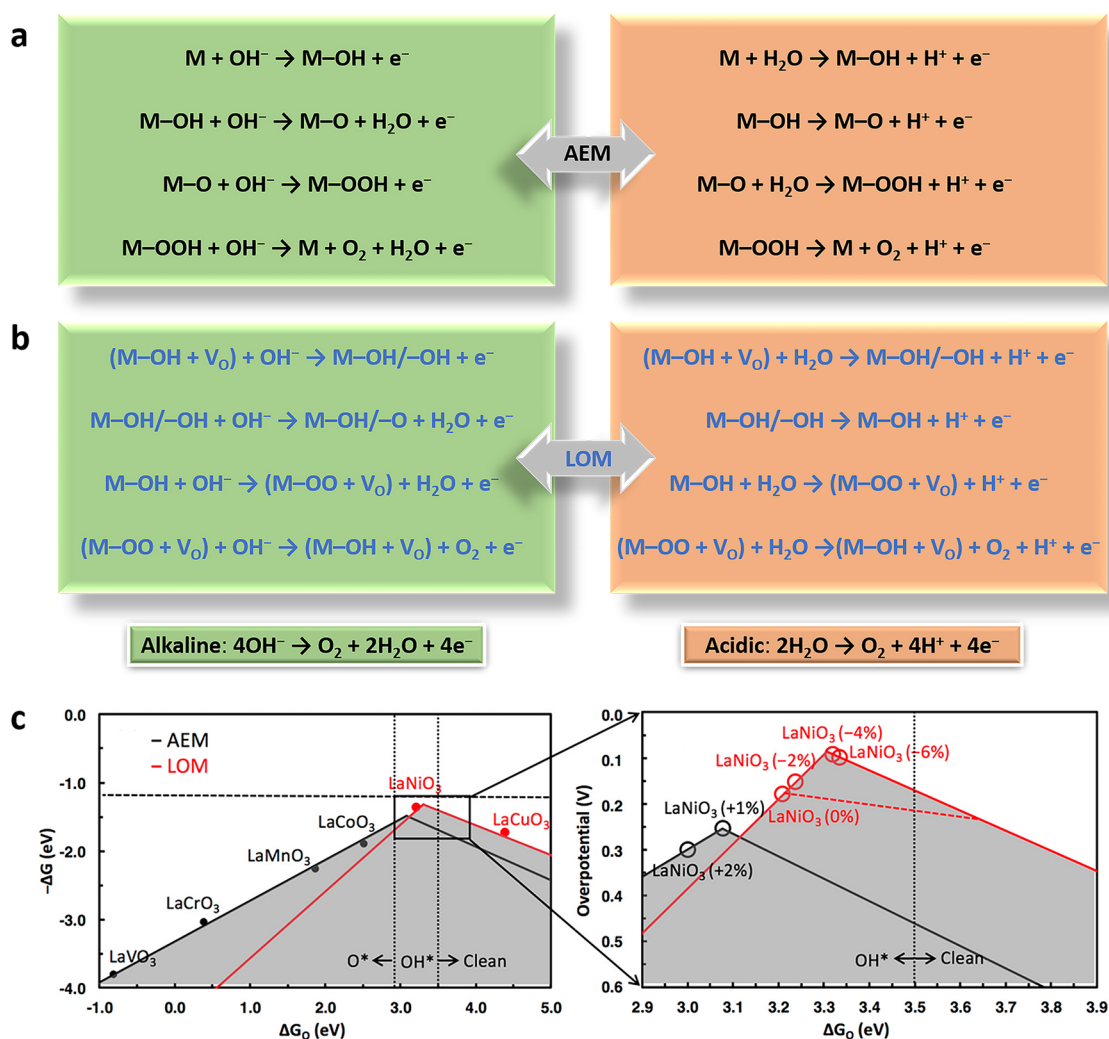
Fig. 1 Reaction pathways for the OER in acidic and alkaline media via **a** AEM, and **b** LOM. **c** The overall OER activity volcano considers both AEM (black) and LOM (red) [97]

in alkaline electrolytes (Fig. 1b), the hydroxyl is adsorbed on the oxygen vacancy-coordinated metal site. Then, another hydroxyl adsorbs at the V_O site, following a dehydrogenation step. The hydroxyl is difficult to dehydrogenate directly, resulting in the formation of a transition state. Finally, the original state $M-OH/-V_O$ is regained after releasing the oxygen and filling the hydroxyl. The acidic LOM process is like the alkaline one, with the main difference being the absence of OH^- and the creation of H^+ in each stage. The oxygen from the catalyst engages directly in OER in the LOM process, resulting in more effective catalysis.

A fundamental contrast between LOM and AEM is the origin of the oxygen molecules, which are created not only from water molecules but also from lattice oxygen of the oxides [78]. LOM is thought to be more effective than AEM [97, 101], because AEM is restricted by the theoretical potential (0.37 V), but LOM with direct O–O coupling can avoid scaling relation limits [78]. It should be noted that entirely denying AEM is not realistic. AEM is constrained by the oxygenated intermediates, which has prompted the investigation on LOM. LOM, on the other hand, is often associated with significant V_o formation and metal dissolution, resulting in unstable crystals, whereas AEM catalysts, in theory, do not experience this extreme surface reconstruction [102]. AEM and LOM frequently occur concurrently, creating conflict between these two systems. As a result,

balancing stability and activity in OER remain an important challenge in the quest to discover efficient and stable catalysts. Recently, in ABO_3 electrocatalysts, adjusting the B-site metals, enhancing the covalency of metal–oxygen, and generating bulk oxygen vacancies were shown to improve the process of transition from the AEM mechanism to the LOM mechanism [89]. Moreover, Kolpak's group explored a range of perovskite catalysts, such as $LaVO_3$, $LaCrO_3$, $LaMnO_3$, $LaCoO_3$, $LaNiO_3$, and $LaCuO_3$, to study the theoretical overpotential (Fig. 1c) [97]. AEM is ubiquitous in the OER activity volcano trend on ABO_3 perovskites, but LOM is reliant on A cation sites.

2.2 Reaction Mechanism of Oxygen Reduction

Although the ORR has been extensively studied in conjunction with the creation of fuel cells, the precise reaction mechanism is still being debated [103]. Figure 2a depicts the overall four-electron reaction. The first electron transfer steps to adsorbed oxygen species, with or without fast proton transfer, are commonly recognized as the RDS on noble metal (e.g., commercial Pt-containing) catalyst surfaces. The initial electron transfer step to O_2 ($O_2 + e^- \rightarrow O_2^-$) is surface sensitive, which displaces H_2O from the electrode surface and inhibits the formation of HO_2^- species. O_2 is a stable molecule before decomposing into O_2^- and HO_2^-; thus, it may be observed in the cyclic voltammograms via reverse sweep. The pH changes resulted in a drop in the overpotential from 1.53 to 0.7 V with pH values changing from 0 to 14 for O_2/O_2^-, whereas the standard reduction potential decreased from 1.229 to 0.401 V for H_2O/OH^-. Conversely, the ORR reaction pathways on transition metal oxide surfaces follow a different logic than those on precious metal surfaces. To achieve total oxygen coordination, surface cations of transition metal oxides interact with the oxygen of H_2O. The hydrogen atoms of H_2O are spread throughout the catalyst surface, as the protonation is charge compensated by the reduction of cation at surface such as Fe^{3+}, Co^{3+}, Mn^{4+}, to produce OH^- (Fig. 2b). Inorganic chemistry concepts help explain the interaction of oxide catalysts with O_2 such as crystal field theory and molecular orbitals [104].
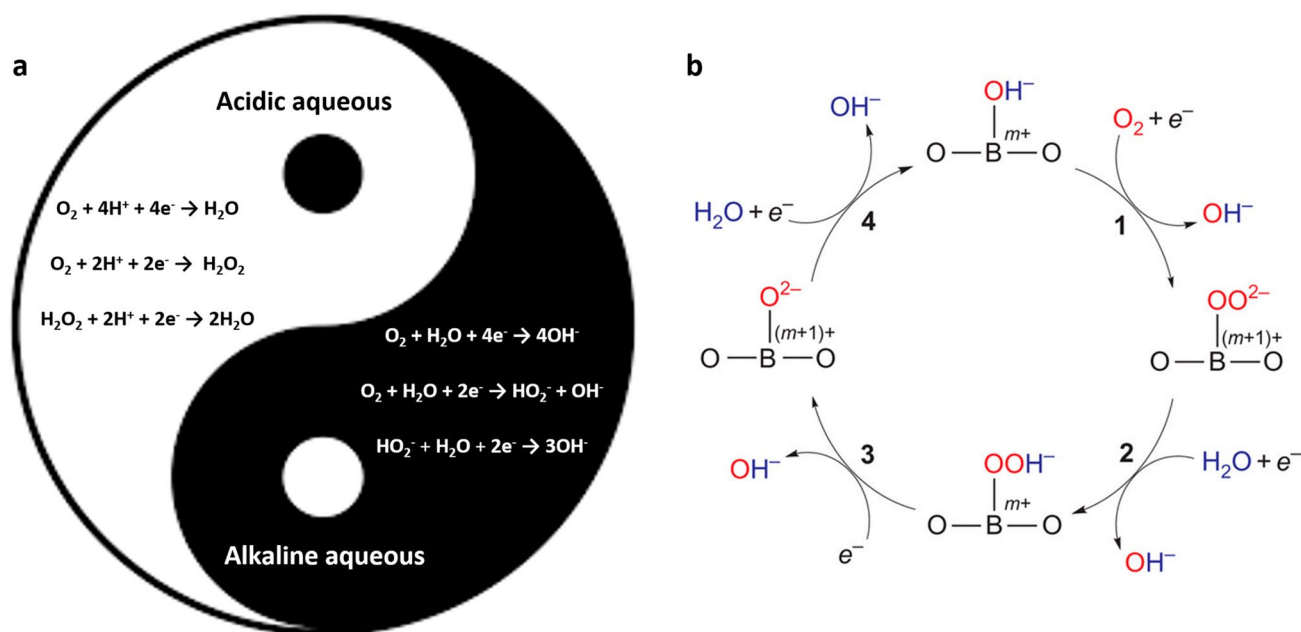

Fig. 2 **a** Normal reaction pathways for the ORR in acidic and alkaline media. **b** Proposed ORR mechanism on oxide catalysts. The ORR process via four steps: 1, surface hydroxide displacement; 2, surface peroxide formation; 3, surface oxide formation; 4, surface hydroxide regeneration [104]

3 Overview of Oxide Catalyst for Oxygen Electrocatalysis

The development of active, low-cost oxygen electrocatalysts is crucial to addressing the efficiency issue. The catalyst design must be predicated on a solid understanding of the OER and ORR mechanism and the source of the reaction over potential. The development of high-performance electrocatalysts follows the four general principles: abundant electroactive sites; high intrinsic catalytic activity; high electrical conductivity; long-term performance stability (Fig. 3). Based on these principles, it is possible to screen catalyst candidates by regulating the electronic structure [83], morphology [105, 106], crystallinity [107], foreign elements doping into the lattice [35, 108], vacancies [109], strains [110, 111], e_g orbital occupancy [69, 104, 112], metal–oxygen covalency [45, 113], controlling and engineering the interface [114, 115], etc. Moreover, controlling the reaction path of OER/ORR would directly adjust the OER/ORR performance, for example adjusting the redox chemistry of lattice oxygen anions to balance the proportion of LOM and AEM would facilitate the OER process [89, 116].

3.1 Substitution of Foreign Elements

It is well known that introducing heteroatoms is a simple and efficient way to accelerate sluggish reaction kinetics [117, 118]. Table 1 summarizes the substitution of foreign elements for the oxygen electrocatalysis. Doping changes the binding energy of intermediates such as *O–OH, *OH, and *O by modifying the electronic structure. As a result, as compared to alternative ways for enhancing OER/ORR activities, doping provides an efficient means of achieving long-term stability with large-scale activity. By integrating extra elements, doping produces ionizable species inside the host material. The ionizable species may cause a change in the Fermi level (E_F), allowing for better catalytic activity in carrier transport [119]. Nowadays, the current commercial ORR catalyst is still Pt/C, while commercial acidic OER catalysts are mainly RuO_2 and IrO_2. Thus, catalysts are usually compared to these commercial catalysts as standard from activity and durability aspects. In this section, we will go through the effects of doping strategy in the oxide catalysts for oxygen electrocatalysis.

Researchers doped RuO_2 with a trace of Ir ($Ru_xIr_{1-x}O_2$) and discovered a considerable gain in stability while compromising OER performance [131]. Earth abundant metals substitution such as Co [132], Cu [121, 133], Mn [122], Ni [132], Ce [123], Mg [124], W [134], Cr [120], and Zn [135] is another method of increasing OER activity with reduced overall noble metal concentration. For instance, after Cu doping, $Cu_{0.3}Ir_{0.7}O_\delta$ exhibited enhanced OER activity in acidic, neutral, and alkaline conditions compared to pure IrO_2 [133]. It was determined that increasing the Jahn–Teller
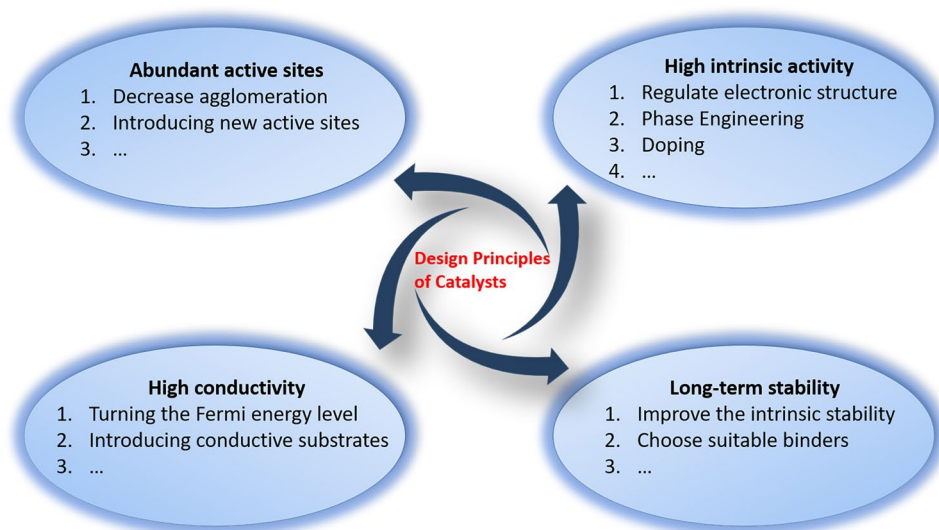

Fig. 3 Design principles of oxide electrocatalysts for OER/ORR

Table 1 Representative summary of substitution of foreign elements for the oxygen electrocatalysis

| Catalyst	Foreign element	Applications	Electrolyte	Performance	Refs
NiCoFeO	Fe	OER	1 M NaOH	1.43 V vs. RHE at 10 mA cm^{-2}	[117]
Cr$_{0.6}$Ru$_{0.4}$O$_2$	Cr	OER	0.5 M H$_2$SO$_4$	1.41 V vs. RHE at 10 mA cm^{-2}	[120]
Cu-RuO$_2$	Cu	OER	0.5 M H$_2$SO$_4$	1.42 V vs. RHE at 10 mA cm^{-2}	[121]
Mn-RuO$_2$	Mn	OER	0.5 M H$_2$SO$_4$	1.39 V vs. RHE at 10 mA cm^{-2}	[122]
Ce$_x$-IrO$_2$	Ce	OER	0.5 M H$_2$SO$_4$	1.45 V vs. RHE at 10 mA cm^{-2}	[123]
Mg-RuO$_2$	Mg	OER	0.5 M H$_2$SO$_4$	1.46 V vs. RHE at 10 mA cm^{-2}	[124]
La$_{0.6}$Sr$_{0.4}$CoO$_3$	Sr	OER	0.1 M KOH	1.53 V vs. RHE at 0.19 mA mg$_{oxide}^{-1}$	[125]
La$_{0.3}$–5582	La	OER and ORR	0.1 M KOH		[126]
PrBa$_{1-x}$Sr$_x$Co$_2$O$_{5+\delta}$	Sr	OER and ORR	0.1 M KOH	1.52 V vs. RHE at 10 mA cm^{-2} for OER; 0.75 V vs. RHE, onset potential for ORR	[127]
YCR	Co	OER	0.5 M H$_2$SO$_4$	1.50 V vs. RHE at 10 mA cm^{-2}	[128]
Sr$_{0.95}$Ce$_{0.05}$Fe$_{0.9}$Ni$_{0.1}$O$_3$	Ce/Ni	OER	0.1 M KOH	1.57 V vs. RHE at 10 mA cm^{-2}	[129]
Co-RuO$_2$	Co	OER and ORR	0.1 M KOH	1.49 V vs. RHE at 10 mA cm^{-2} for OER; 0.82 V vs. RHE, half-wave potential for ORR	[130]
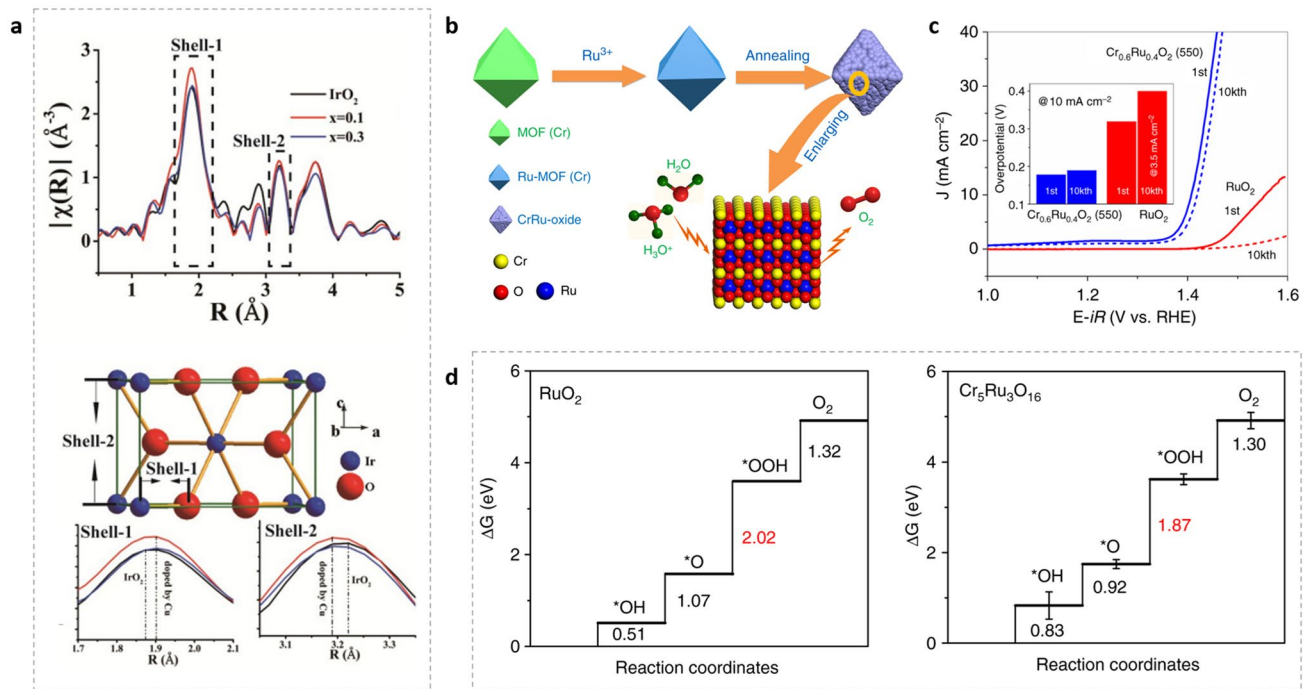
Fig. 4 **a** Fourier transforms of the k 3 -normalized Ir-LIII edge EXAFS for Cu$_x$Ir$_{1-x}$O$_\delta$ compositions (up), and the sketch of one unit cell of IrO$_2$ (up). The shell-1 formed due to an Ir-O bond, and shell-2 formed due to an Ir-Ir bond [133]. **b** The synthesis of Cr$_{0.6}$Ru$_{0.4}$O$_2$ electrocatalysts for OER use in acid conditions is depicted schematically. **(c)** LSVs of Cr$_{0.6}$Ru$_{0.4}$O$_2$ (550) and commercial RuO$_2$ for the first and 10,000th cycle. **d** The calculated free energy diagrams for RuO$_2$ and Cr$_5$Ru$_3$O$_{16}$ [120]

effect in the IrO$_6$ and CuO$_6$ octahedral (Fig. 4a) structure would enhance the lift degeneracy of the e$_g$ and t$_{2g}$ orbitals and thus improve the catalysis performance. It minimizes the gap in free energy between ΔG_2 and ΔG_3 from density

functional calculations (DFT), resulting in a reduced theoretical overpotential compared to IrO$_2$ [133]. Recently, Chen's group reported metal–organic framework (MOF)-derived Cr$_{0.6}$Ru$_{0.4}$O$_2$ for acidic OER [120]. RuCl$_3$ was first loaded

into the pores of MIL-101 (Cr) by impregnation. The resulting RuCl$_3$-MIL-101 (Cr) was annealed in air for 4 h between 450 and 600 °C to produce Cr$_{0.6}$Ru$_{0.4}$O$_2$ catalyst (Fig. 4b). Cr$_{0.6}$Ru$_{0.4}$O$_2$ (550 °C) displays not only excellent OER activity, but also strong stability with only 11 mV overpotential decrease after 10,000 cycles at 10 mA cm^{-2} (Fig. 4c). DFT simulations showed an additional mechanism for the high OER performance. The RDS at the Ru site on the Cr$_5$Ru$_3$O$_{16}$ surface was determined to be 1.87 eV, 0.15 eV lower than RDS on the RuO$_2$ (2.02 eV) (Fig. 4d) [120].

It is also a universal strategy via doping for perovskite-like oxides to improve the OER/ORR activity and stability [75, 80]. The standard perovskite with the general formula ABO$_3$, where A is either an alkaline earth metal or a rare earth metal, and B is a transition metal, is widely investigated according to doping strategy for oxygen electrocatalysis. Doping at the A-site, B-site, or even O-site to induce oxygen vacancies, which adjust the electronic structure of other parts in the perovskite, can be used to modify the OER/ORR activity. The oxidation state of transition metal affects metal–oxygen hybridization; therefore, the electronic behaviors of these perovskites depend on this parameter. Strongly electronegative transition metals exhibit high metal–oxygen hybridization, and the d-band center of the transition metal oxide gets closer to O 2p states as the electronegativity increases. However, in addition to metal–oxygen hybridization, cation doping also brings other effects on octahedral tilting and Jahn–Teller distortion, which all play important roles in determining the electrical characteristics of perovskite oxides [136, 137]. The A-site is not commonly regarded as the active site directly involved in the oxygen electrode processes. However, A-site cations may have an indirect effect on the perovskite's ORR/OER performance. Sr replacements in La$_{1-x}$Sr$_x$CoO$_3$ are found to straighten the octahedral cage, align atoms along the Co–O–Co axis (Fig. 5a), and increase the average oxidation state of the Co cations (Fig. 5b). As a result, both electrical conductivity and activity toward the OER are significantly enhanced (Fig. 5c). According to DFT, the alignment of the Co–O–Co bonds and the oxidation of the Co cations enhance the overlap between the occupied O 2p valence bands and the unoccupied Co 3d conduction bands, explaining why conductivity improves as the amount of Sr increases [125]. Doping the Sr site with Na (Sr$_{1-x}$Na$_x$RuO$_3$) improves the activity and durability of SrRuO$_3$ perovskite, resulting in a decrease in octahedral distortion and an increase in the oxidation state

(Fig. 5d) [138]. Although SrRuO$_3$ binds reaction intermediates too strongly, Na doping of 12.5 at% leads in nearly optimal OER activity. The addition of Na increases the oxidation state of Ru, displacing positively charged O p-band and Ru d-band centers and weakening Ru-adsorbate bonds (Fig. 5e). The increased stability of Na-contained perovskites is due to the stability of Ru centers, which results in somewhat higher oxidation states, lower surface energy, greater dissolving potentials, and less deformed RuO$_6$ octahedra [138]. In addition to the cations doping with lower valence, the cations with higher valence are also active for oxygen electrocatalysis. Recently, it has been reported that doping La into the A-site of BSCF5582 selectively causes local stress on the Co sublattice octahedron, which lead to a better ORR and OER performance [126]. From the EXAFS data (Fig. 5f), the peak intensities of La$_{0.3}$–5582 are shown to be significantly higher than those of BSCF5582 in all atomic edges, indicating that La-doping promotes the stretch-up of atomic arrangement in the lattice. Meanwhile, the peak of the Co K-edge is divided into two peaks with different r spaces. It is reasonable to claim that the selective impact of the La-doping can cause local stress on the unit cell of the Co sub-lattice in a cubic perovskite structure, while the unit cell of the Fe-site sub-lattice is less affected, causing the simultaneous appearance of rhombohedral LaCoO$_3$ aggregates and the comminution of particles (La doped BSCF5582) into smaller ones (Fig. 5g) [126]. In other words, the dynamic microstructure phenomena are caused by the implantation of A-site cations with La^{3+} (charge imbalance) and local stress on the Co-site sub-lattice with the cubic perovskite structure. After La-doping, the synthesized La$_{0.3}$(Ba$_{0.5}$Sr$_{0.5}$)$_{0.7}$Co$_{0.8}$Fe$_{0.2}$O$_{3-\delta}$ displayed excellent OER and ORR performance (Fig. 5h, i) [126]. Another effective higher valence ion is Co^{4+}, which has been shown to possess good electrophilicity [139]. The OER activity of the perovskite is enhanced by the electrophilic surface Co^{4+}, which makes it easier to generate surface O-OH and deprotonate surface-adsorbed OOH* species via an inductive, electron-withdrawing effect [139]. Adjusting the electronic surface structure of catalysts via doping can improve the non-electrochemical steps (adsorption and desorption processes) [104], of PrBa$_{1-x}$Sr$_x$Co$_2$O$_{5+\delta}$ in which the surface-accumulated Co^{4+} was found to promote both OER and ORR as an excellent bi-functional catalyst [127]. The doping strategy is an effective method to adjust the surface structure of catalysts and then affect the interactions because of the modulated electron unsaturated state,
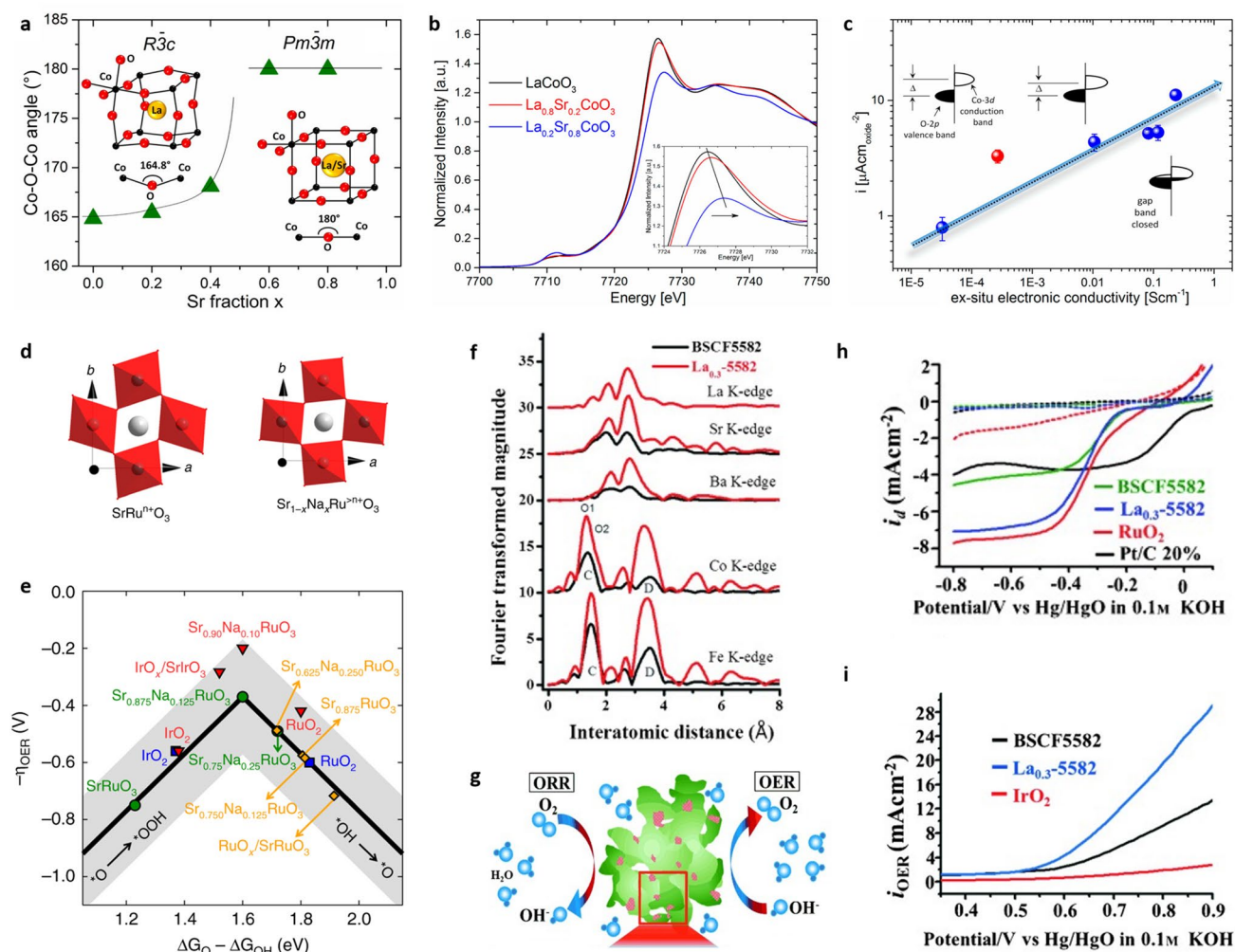
Fig. 5 **a** Evolution of Co–O–Co angle as a function of the Sr fraction [125]. **b** Co K-edge XANES spectra of the $La_{1−x}Sr_xCoO_3$ at room temperature [125]. **c** Current density ($\mu A\ cm_{oxide}^{−2}$) as a function of the ex situ electronic conductivity of the $La_{1−x}Sr_xCoO_3$ series; the red circle represents the $SrCoO_{2.5}$ [125]. **d** Octahedral distortion in $SrRuO_3$ compared to Na-doped $Sr_{1−x}Na_xRuO_3$ [138]. **e** OER Volcano-type activity plot [138]. **f** The radial distribution function for the all atomic EXAFS spectra for BSCF5582 and $La_{0.3}$–5582. **g** The rhombohedral phase $LaCoO_3$ grains are separated on the surface of cubic-based grains of parent $La_{0.3}$–5582. LSV of **h** ORR and **i** OER on BSCF5582 and $La_{0.3}$–5582 compared to commercial catalysts [126]

for example, high oxidation status of metals sites displaying higher electrophilicity and stronger absorption efficiency/weaker desorption efficiency for OH⁻.

3.2 e_g Orbital Occupancy

Because the B-site directly participates in oxygen redox reactions, B-site substitution is a straightforward and effective way for regulating the ORR/OER activity of a perovskite catalyst [140, 141]. The discovery of a catalyst design approach that links material properties to catalytic activity

by Shao-Horn's group speeds up the search for highly active and cheap transition-metal-oxide catalysts to replace precious metal catalysts (Ru, Ir, Pt) [104, 142]. The intrinsic OER activity of surface transition metal cations in an oxide exhibits a volcano-shaped dependence on 3d electron occupancy with an e_g symmetry. The best OER activity was predicted to occur at close to unity e_g occupancy, with strong covalency of transition metal–oxygen links (Fig. 6a) [142]. Shao-Horn's group demonstrates that the ORR activity of oxide catalysts is mostly related to the B-site metal–oxygen covalency, which serves as a secondary activity descriptor (Fig. 6b) [104]. Xu's group did further descriptor work on
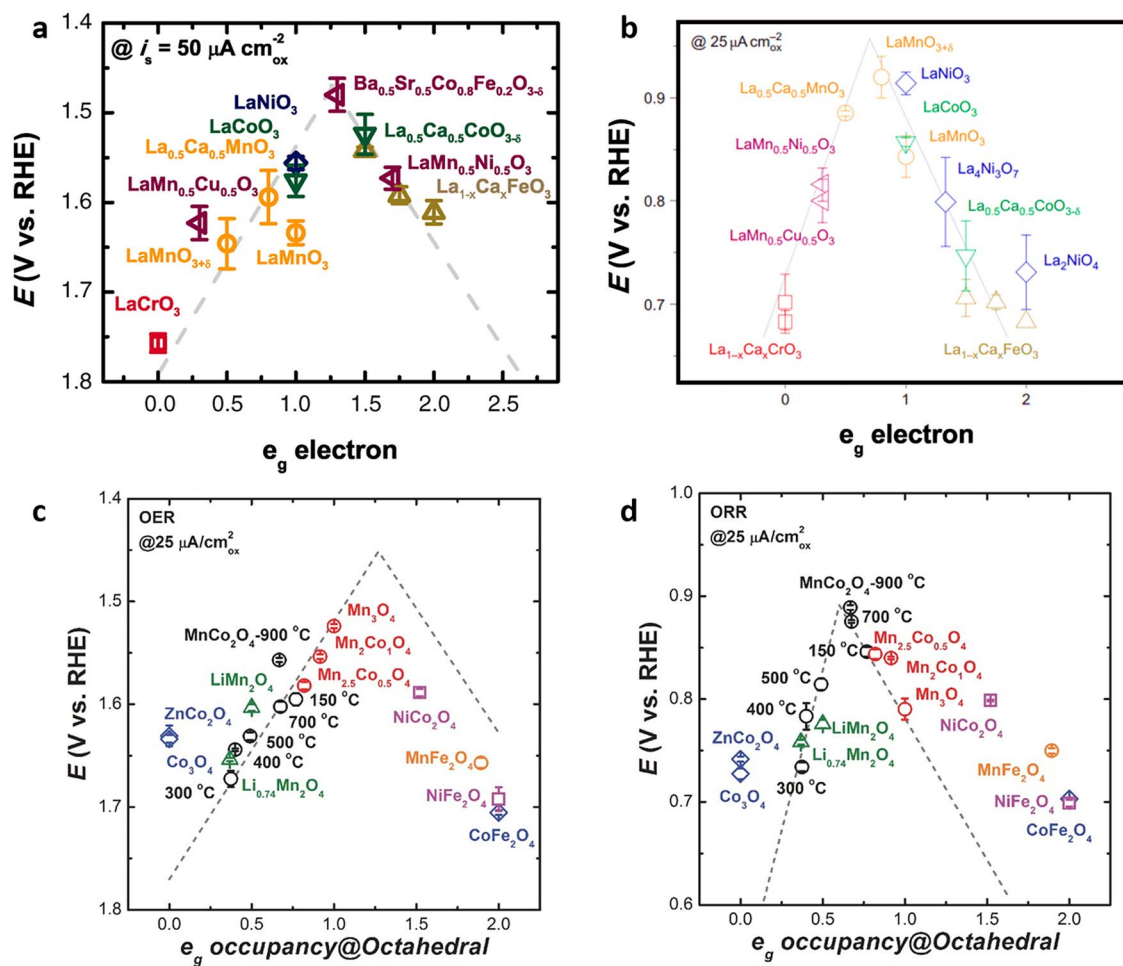
Fig. 6 The relation between the **a** OER and **b** ORR catalytic activities and the occupancy of the e_g-symmetry electron of the perovskite oxides [104, 142]. OER activity defined by the overpotentials at 50 μA cm_{oxide}^{-2} of OER current; ORR activity defined by the overpotentials at 25 μA cm_{oxide}^{-2} of ORR current. **c** OER and **d** ORR activity on various spinel oxides as a function of e_g occupancy of the active element at octahedral site [74]

OER and ORR of spinel oxides, including $Mn_xCo_{3-x}O_4$, XCo/Fe_2O_4, and Li_xMn_2O [74]. The e_g occupancy of the active cation at the octahedral site is the activity descriptor for spinels' ORR/OER, confirming the relevance of electron orbital filling in metal oxide catalysis (Fig. 6c, d) [74]. When two distinct cations occupy the same octahedral site, the e_g values is utilized. There is a four-step proton/electron-coupled reaction mechanism [143, 144], in which the binding strength of OER/ORR reaction intermediates is governed by e_g filling [104, 142]. The electrocatalysis activity of spinel oxides is summarized and compared to the e_g occupancy as-extracted. For instance, octahedral element filling and active element occupancy at the octahedral site simultaneously determine oxygen electrocatalysis

performance, demonstrating the usefulness of this paradigm (e_g occupancy) to unify the ORR/OER activity prediction of spinel oxides (Fig. 6c, d) [74]. Changing the oxidation state [90, 145–147], or the spin state [148, 149] of a transition metal can control the e_g orbital occupation of its 3d electrons in the octahedral site.

Shao's group developed $SrM_{0.9}Ti_{0.1}O_3$ with different B-site transition metal elements for OER [150]. Both $SrCo_{0.9}Ti_{0.1}O_3$ (SCT) and $SrFe_{0.9}Ti_{0.1}O_3$ (SFT) exhibit enhanced OER activities compared to the original spinel, and also comparable to the $Ba_{0.5}Sr_{0.5}Co_{0.8}Fe_{0.2}O_3$ (BSCF). SCT demonstrated greater operational stability than SFT, outperforming BSCF and IrO_2 catalysts [150]. It was explained by the e_g filling which is 1.16 close to

the standard 1 and the formation of redox-active oxygen deficiency [142]. Ciucci's group introduced Nb into the Mn site of CaMnO$_3$ (CMO) and treated the material with H$_2$ to prepare CaMn$_{0.75}$Nb$_{0.25}$O$_{3-\delta}$ (H$_2$-CMNO) which displayed dramatically enhanced OER/ORR activity compared to CMO [151]. This significant increase in OER/ORR activity can be attributed to Nb^{5+} doping inducing oxidation state changes on Mn from +4 to +3, which directly optimizes the e$_g$ value close to unity to increase OH– adsorption [151]. Liu's group also synthesized a double perovskite PrBa$_{0.5}$Sr$_{0.5}$Co$_{1.5}$Fe$_{0.5}$O$_{5+\delta}$ nanofiber as an efficient and robust catalyst for OER [152]. The co-doping strategy of Sr and Fe into PrBCo$_2$O$_{5+\delta}$ is shown to be particularly successful in increasing the intrinsic activity about 5 times, which could be attributed to the favorable e$_g$ electron filling. Shui's group reported a hexagonal perovskite, BaNiO$_3$ as a catalyst for OER in

alkaline media, with an activity one order higher compared to IrO$_2$ [146]. The underlying mechanism results from structural transition from BaNiO$_3$ to BaNi$_{0.83}$O$_{2.5}$ (Ba$_6$Ni$_5$O$_{15}$) throughout the OER cycle process (Fig. 7) [146]. The calculated e$_g$-orbital fillings are 0 for BaNiO$_3$ (Ni^{4+} (t$_{2g}$)^6(e$_g$)^0), 2 for BaNiO$_2$ (Ni^{2+} (t$_{2g}$)^6(e$_g$)^2), and 1.4 for BaNi$_{0.83}$O$_{2.5}$ (Ni^{2+} (t$_{2g}$)^6(e$_g$)^1, Ni^{3+} (t$_{2g}$)^6(e$_g$)^1, and Ni^{4+} (t$_{2g}$)^6(e$_g$)^2), respectively (Fig. 7a–c) [146]. It agrees well with the principle put forward by Shao-Horn's group [142], as BaNi$_{0.83}$O$_{2.5}$ displays the best OER activity and BaNiO$_3$ the worst (Fig. 7d). The free energy diagrams of the BaNiO$_3$, BaNi$_{0.83}$O$_{2.5}$, and BaNiO$_2$ are shown in Fig. 7e. The underlying mechanism resulting in the highest OER activity of BaNi$_{0.83}$O$_{2.5}$ is as follows: the difference in free energies between OO* and HOO* on BaNi$_{0.83}$O$_{2.5}$ is maximized among the three perovskite oxides, as reflected by the smallest overpotential [146].
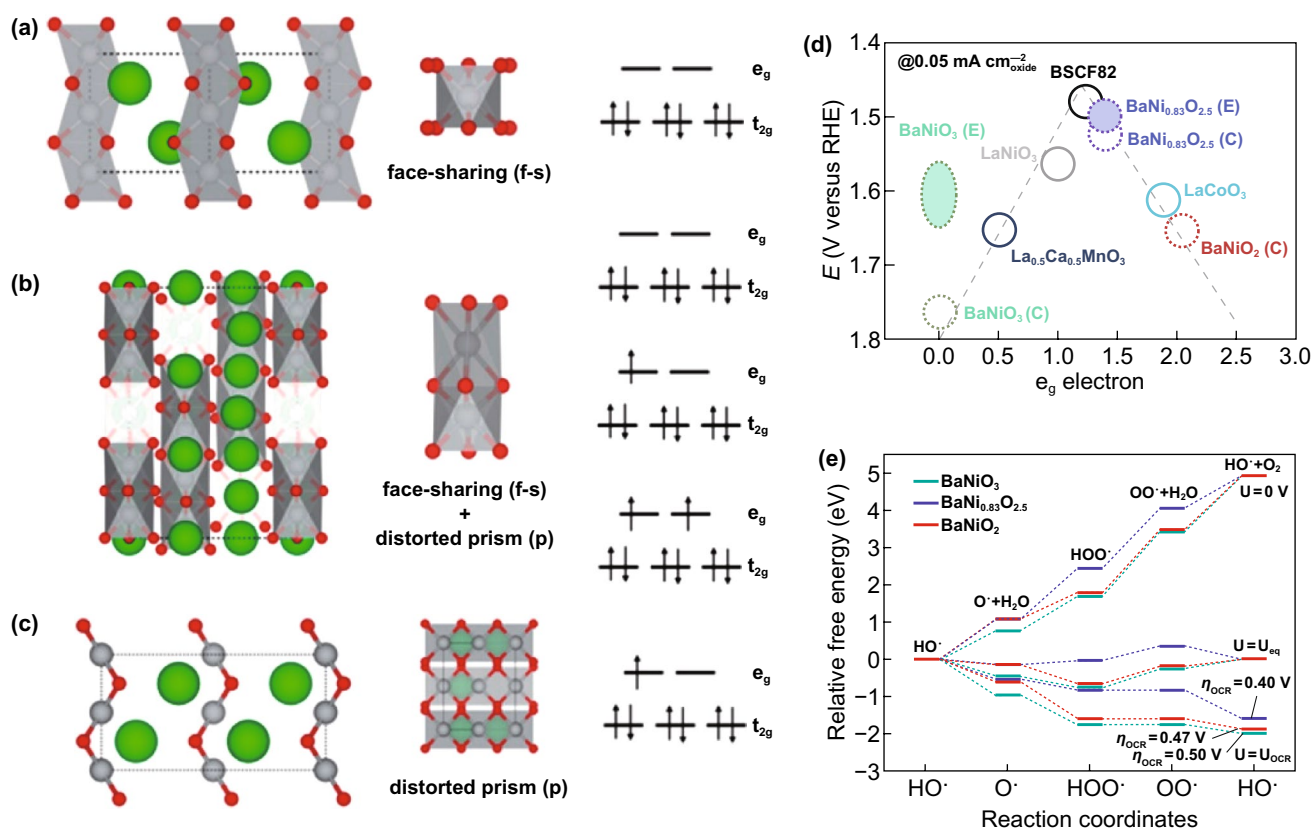

Fig. 7 Schematics of phase transformation and the evidence of the OER activity of the BaNiO$_3$. **a** Schematic of the BaNiO$_3$ crystal structure with the interatomic distances calculated by DFT. **b** Schematic of the BaNi$_{0.83}$O$_{2.5}$ crystal structure with the interatomic distances calculated by DFT. **c** Schematic of the BaNiO$_2$ crystal structure with the interatomic distances calculated by DFT. **d** The relation between the OER catalytic activity, defined by the overpotential at 0.05 mA cm$^{-2}_{oxide}$, of OER current, and the occupancy of the e$_g$ electron of the transition metal. **e** Free energy diagrams of the BaNiO$_3$, BaNi$_{0.83}$O$_{2.5}$, and BaNiO$_2$ depending on the reaction coordinates [146]

3.3 Vacancies

Defect engineering is a known strategy to design more active electrocatalysis for OER [153–155], hydrogen generation [55, 156], ORR [103, 157–159], nitrogen reduction reaction (NRR) [160, 161] and CO_2 reduction (CRR) [162]. Another method for increasing OER activity and stability in acidic media is to produce defect-containing RuO_2 by doping and dopant leaching. Cu-doped RuO_2 porous nano-polyhedra generated from organic frameworks is likely one of the greatest examples of increasing OER activity via the production of oxygen vacancies (Fig. 8a) [121]. The bulk of the oxygen vacancies generated near Cu causes the adjacent Ru atom to become more negative and, as a result, shift the center of the O $2p$ band towards the Fermi level for greater OER activity. Tian et al. synthesized Zn-doped RuO_2 and leached it out in acid to prepare ultrafine defective RuO_2 (named UfD-RuO_2/CC) (Fig. 8b), and the resulting catalyst demonstrated outstanding OER performance in acidic environments with 179 mV overpotential and 20 h stability at a current density of 10 mA cm^{-2}. The strong catalytic activity is attributed to the synergistic impact of active sites and electronic structural tailoring (Fig. 8c) [135]. A cobalt-doped oxygen-defect Ru-based catalyst with 169 mV overpotential and 50 h endurance at 10 mA cm^{-2} current density was recently created. The significant increase in OER performance is attributable mostly to the oxygen vacancies and the changed electronic structure of the Co-doped RuO_2, which employs a vacancy-related LOM path rather than an AEM path. To explore the role of oxygen vacancies in OER, the effect of oxygen vacancies on neighboring Ru atoms was investigated. The optimal lower free energy method was explored by comparing two competing OER processes via O_V^I in LOM and 5-coordinated Ru in AEM (Fig. 8d). In both processes, five elementary steps are considered, including four electrochemical electron transfer steps ($\Delta G_1 \sim \Delta G_4$) and also the non-electrochemical O_2 desorption step (ΔG_5). For the first adsorption of the incoming H_2O molecule, the intermediate L1 (O_V^I–OH) in LOM and intermediate A1 (Ru–OH) in AEM were generated on O_V^I and 5-coordinated Ru sites, respectively. The fact that L1 had a lower adsorption energy than A1 indicates that H_2O preferred to react with the O_V^I vacancy rather than the Ru site [163]. Due to the lower electron depletion of O_V^I vacancy after binding to H_2O, the following OER steps will process in LOM mechanism (Fig. 8e). Moreover, the effect of O vacancy on OER process was also further investigated

on the rate-determining step (RDS) in both LOM and AEM (Fig. 8f). Also, the presence of O vacancies prevents the over-oxidation of Ru to soluble RuO_4, which is thought to be the primary cause of the acidic instability of RuO_2 electrocatalysts regulated by AEM [163].

Creating an A-site shortage in spinels is one method of creating oxygen vacancies to boost oxygen electrocatalysis [164]. Shao's group presented a simple and effective method for creating A-site cation deficiency into $LaFeO_3$ perovskite to increase ORR and OER electrocatalytic activity in alkaline solutions, but the enhancement is more significant for OER than for ORR (Fig. 9a, b) [148]. The increase is due to the formation of surface oxygen vacancies and a trace amount of Fe^{4+} species, as proven via XPS as the slight positive shift of Fe $2p_{3/2}$ peak could be observed for $La_{1-x}FeO_{3-\delta}$ suggesting the presence of iron in a higher oxidation state (+4). Mössbauer spectroscopy is sensitive to iron and is commonly used to investigate iron's electrical structure. Furthermore, the pristine LF revealed a single Fe^{3+} sextet component with strong lines in the Mössbauer spectrum, whereas extra Fe^{4+} occurred in the A-site cation deficient $La_{1-x}FeO_{3-\delta}$ [148]. The significance of oxygen vacancy defects, which allow crystalline oxygen to be mobile at the surface of perovskites, has hitherto gone unnoticed. How much the stoichiometry of oxygen in the crystal structure of perovskites deviates from the nominal value of 3 for the formula ABO_3 influences both the lability of surface oxygen and the underlying electronic structure of these materials [165, 166]. The degree of vacancy generation depends on how close together the $2p$ band of oxygen and the $3d$ band of the metal are in the crystal, with more covalent systems displaying larger vacancy concentrations as shown in Fig. 9c [167]. The d orbitals of the Co ion have a higher overlap with the s and p orbitals of the O^{2-} ion as the oxidation state of Co increases, resulting in the creation of the π* and σ* bands. Stevenson's group has introduced a number of cobaltite perovskites in which the covalency of the Co–O bond and the amount of oxygen vacancies are controlled by the substitution of Sr^{2+} into $La_{1-x}Sr_xCoO_{3-\delta}$ [167]. When there is sufficient Co $3d$ and O $2p$ band overlap, vacancies are produced, which is indicative of the underlying electronic structure in the vacancy parameter (Fig. 9d). The vacancy would then affect oxygen diffusion rate, which is directly correlated with OER performance (Fig. 9e) [167]. Another strategy is to create cation deficiencies to adjust the electronic structure of other cations and the overlap of the d orbital of the metal and the $2p$ orbital from oxygen. Jiang et al. synthesized a RuO_2/LFRO composite by
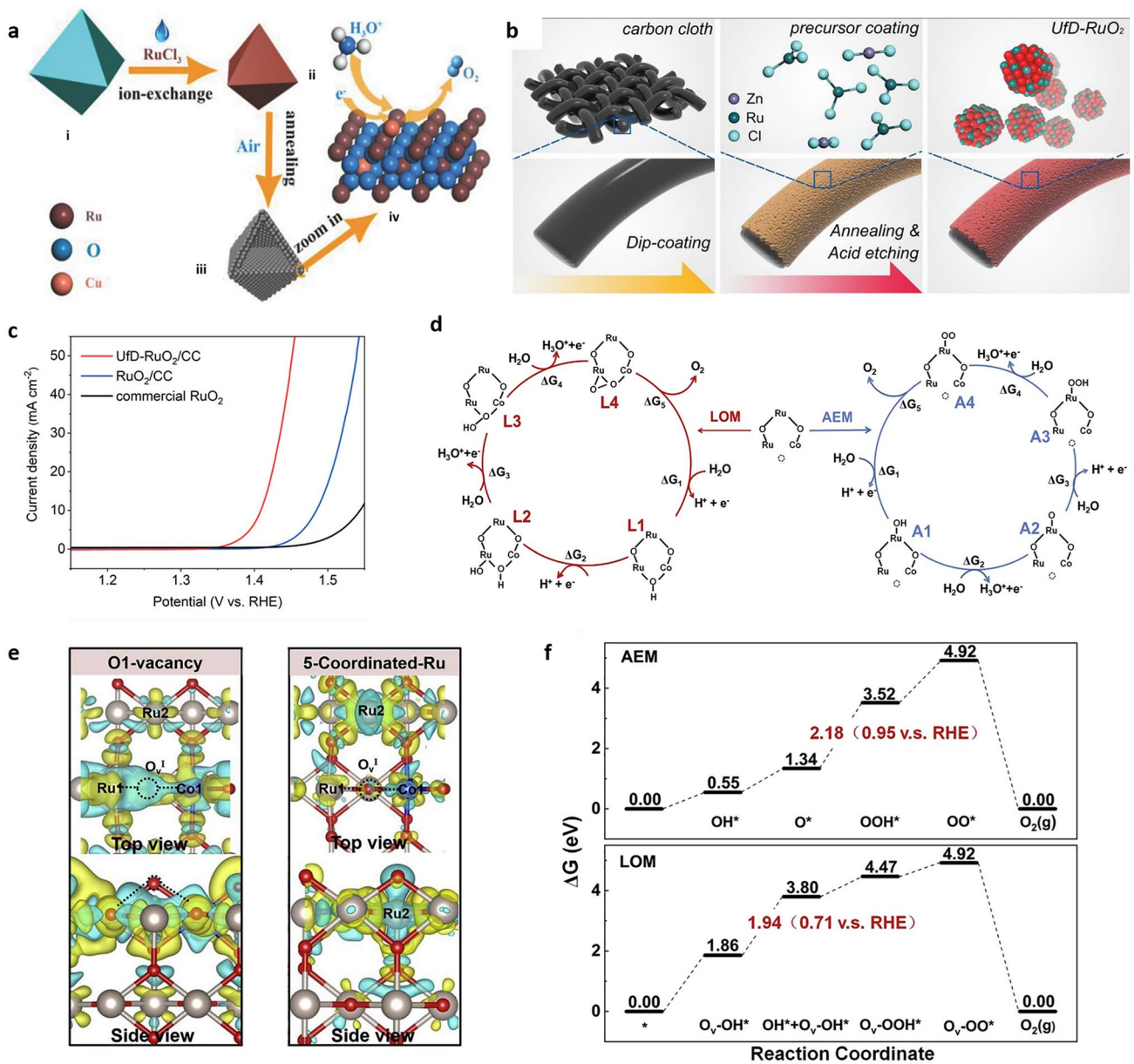
Fig. 8 **a** The synthesis process and model of Cu-doped RuO$_2$ hollow porous polyhedron are depicted schematically. (i) A Cu-BTC polyhedron, (ii) a Ru-exchanged MOF-derivative polyhedron, (iii) a hollow porous polyhedral aggregation of ultrasmall Cu-doped RuO$_2$ nanoparticles, (iv) an expanded model of Cu-doped RuO$_2$ as an electrocatalyst for OER in acidic environments [121]. **b** Illustration of the synthetic route for the UfD-RuO$_2$/CC [135]. **c** OER polarization curves of samples synthesized (UfD-RuO$_2$/CC, RuO$_2$/CC, and commercial RuO$_2$/CC) after capacitance-correction and iR-correction with the same mass loading in O$_2$ saturated 0.5 m H$_2$SO$_4$ solution [135]. **d** Proposed LOM and AEM mechanisms. **e** The charge energy difference of A1 and L1 to illustrate the lower electron depletion on O$_V^I$ than Ru. **f** The free energy diagrams of the two mechanisms of LOM and AEM [163]

the exsolution of a low Ru-substituted A-site deficient perovskite, La$_{0.9}$Fe$_{0.92}$Ru$_{0.08}$O$_3$ (LFRO) [168]. In this procedure, pure Ru NPs are exsolved from LFRO through a heat treatment in 5% H$_2$/Ar at a relatively low temperature (Fig. 9f, g). Next, the exsolved Ru NPs were converted into RuO$_2$ for the oxygen

evolution reaction (OER). In comparison with the pure LFRO, the RuO$_2$/LFRO composite had a strong OER performance, which was primarily due to the production of electrochemically active RuO$_2$ NPs and the enhancement of the electrical conductivity [168]. Furthermore, the exsolution is a reversible
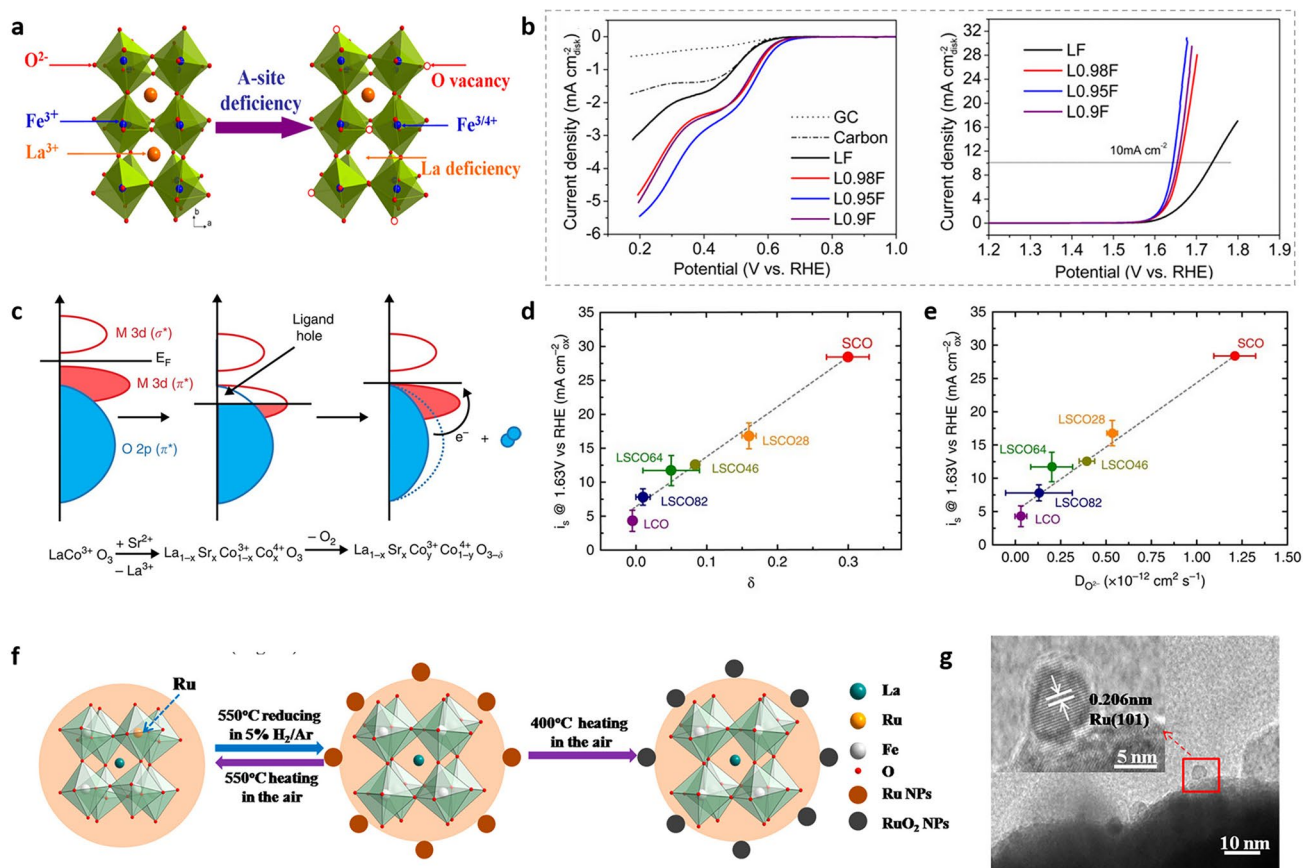
Fig. 9 **a** Schematic illustration of the formation of oxygen vacancy and Fe^{4+} in A-site-deficient $La_{1-x}FeO_{3-\delta}$ perovskites [148]. **b** LSV curves for the ORR and OER on the RDE (1600 rpm) comprised of LF, L0.98F, L0.95F, and L0.9F catalysts in O^{2-}saturated 0.1 M KOH solution [148]. **c** Relationship between oxygen vacancy concentration and Co–O bond covalency in $La_{1-x}Sr_xCoO_3$ [167]. **d** Correlation of oxygen evolution activity with the vacancy parameter δ [167]. **e** Correlation of oxygen evolution activity with the oxygen ion diffusion rate [167]. **f** Lattice structures of LFRO, Ru/LFRO, and RuO_2/LFRO. **g** TEM image of LFRO-550H, inset is the exsolution of a Ru nanoparticle [168]

process, and by heating at 550 °C in air, the exsolved Ru NPs "redissolve" into the perovskite lattice [168]. The in situ exsolution from perovskite oxide catalyst can also be used to synthesize electrocatalysts, for the hydrogen evolution reaction (HER). Zhu et al. reported that the $La_{0.4}Sr_{0.4}Ti_{0.9}O_3$ promoted the water dissociation and in situ generated Ni nanoparticles favor hydrogen adsorption for the recombination into H_2 [169]. Table 2 summarizes some very important references with introducing vacancies for the oxygen electrocatalysis.

3.4 Strain

Strain engineering is an effective method for modifying the metal–oxygen binding energy [39, 171, 172]. The electrical structure can be tuned by lattice strain generated by lattice vacancies, distortion, or mismatch. Tensile strain and

compressive strain are types of lattice strain that, under an octahedral coordination, for instance, promote the filling of in-plane (d_{x2-y2}) and out-of-plane (d_{z2}) orbitals, respectively [25]. Dr. Pesquera's group disclosed the effects of symmetry breaking at free surfaces of ABO_3 perovskite epitaxial films and show that it can be combined with substrate-induced epitaxial strain to tailor at will the electron occupancy of in-plane and out-of-plane surface electronic orbitals [173]. Modifying interatomic lengths has been widely studied in the context of strain engineering. The electronic structure of cubic ABO_3 perovskite is significantly impacted by the octahedral structure, such as B-O bond lengths (Fig. 10a) [172, 174]. Strain has an impact on both the electronic properties and chemical properties. Systematic DFT calculations across the first-row transition metal perovskite oxides in the idealized cubic perovskite structure show that, for early

Table 2 Representative summary of introducing vacancies for the oxygen electrocatalysis

Catalyst	Vacancies	Applications	Electrolyte	Performance	Refs
$Ru_{1-x}O_2$	Ru	OER	0.5 M H_2SO_4	1.41 V vs. RHE at 10 mA cm^{-2}	[135]
$Co_{0.11}Ru_{0.89}O_{2-\delta}$	O	OER	0.5 M H_2SO_4	1.41 V vs. RHE at 10 mA cm^{-2}	[163]
$La_{0.8}Sr_{0.2}CoO_{3-\delta}$	O	OER	0.1 M KOH	8 mA cm$^{-2}_{oxide}$ at 1.63 V vs. RHE	[167]
$SrCoO_{3-\delta}$	O	OER	0.1 M KOH	28 mA cm$^{-2}_{oxide}$ at 1.63 V vs. RHE	[167]
$La_{0.9}Fe_{0.92}Ru_{0.08}O_3$	La	OER	0.1 M KOH	1.65 V vs. RHE at 10 mA cm^{-2}	[168]
$SrFe_{0.9}Si_{0.1}O_3$	O	OER	0.1 M KOH	1 mA cm$^{-2}_{oxide}$ at 1.63 V vs. RHE at	[170]
$SrCo_{0.9}Ru_{0.1}O_3$	O	OER	0.1 M KOH	1.59 V vs. RHE at 10 mA cm^{-2}	[35]
$La_{0.95}FeO_3$	La	OER	0.1 M KOH	1.64 V vs. RHE at 10 mA cm^{-2}	[148]
$La_{0.95}FeO_3$	La	ORR	0.1 M KOH	1.43 mA cm$^{-2}_{oxide}$ at 0.25 V vs. RHE	[148]

transition metals, increasing the d-band width results in a higher d-band center relative to the Fermi level. These calculations assume constant d-band electron filling under strain and approximate the d-band as a rectangular form [175].

However, d-band widening causes a lower d-band center because of the higher d-band filling of late transition metals [175]. For instance, computations on relaxed $La_{0.6}Sr_{0.4}CoO_3$ structures showed that in the region of -3% to 3% biaxial
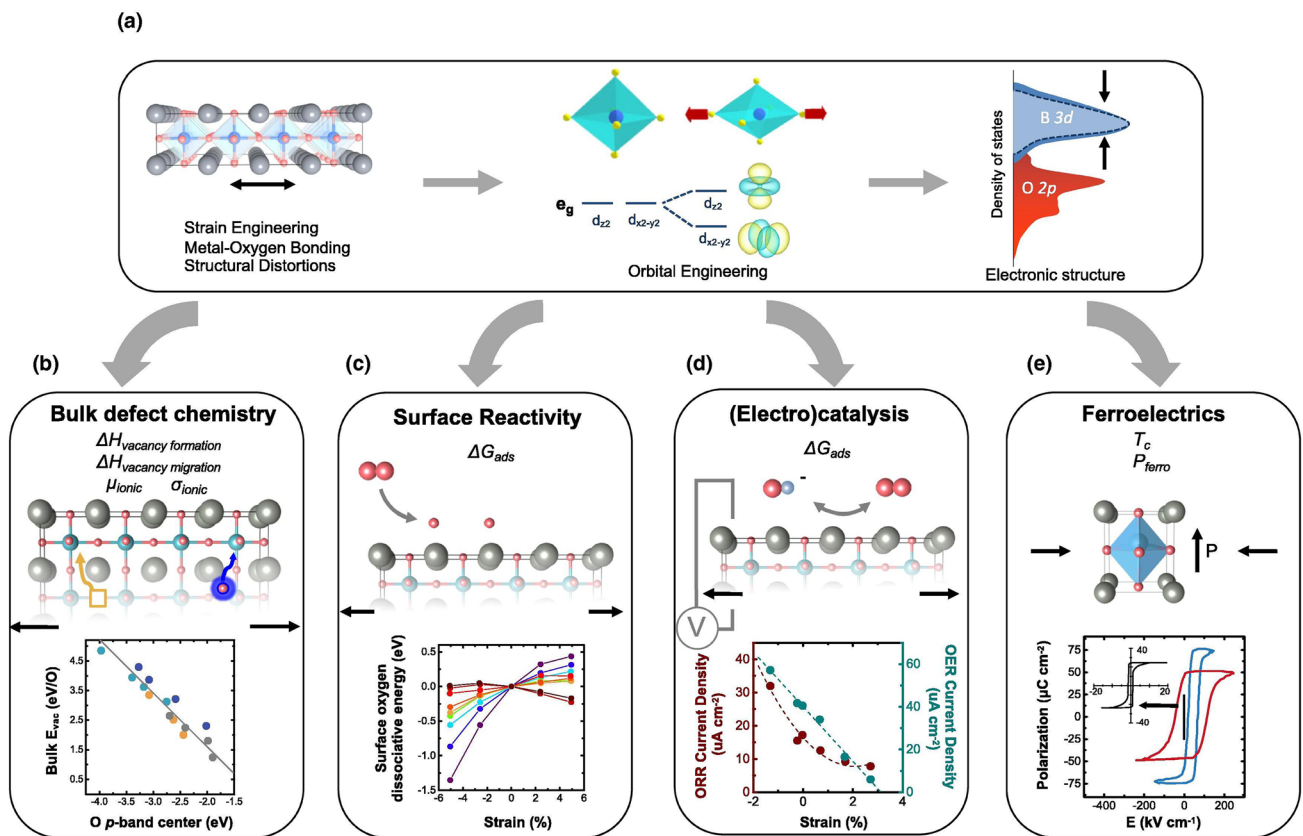

Fig. 10 Interplay between strain in oxides, modification of electronic structure, and the resulting effect on oxide functionalities [172]. **a** Strain-induced structural modification divides previously degenerate energy levels due to symmetry-breaking, whilst changes in metal–oxygen orbital overlap impact the widening of d-states in the electronic density of states [172]. **b** Correlation between raising the oxygen 2p-band center and decreasing the bulk oxygen vacancy formation energy in perovskite oxides [177]. **c** Dependence of the oxygen dissociation energy for the BO_2-terminated lanthanides [175]. **d** Relationship between the room temperature ORR at 0.823 V_{RHE} and OER at 1.623 V_{RHE} for $LaNiO_3$ under various strain effects in 0.1 M KOH [110]. **e** Polarization behavior of single-crystal $BaTiO_3$ versus $BaTiO_3$ grown on $DyScO_3$ and $GdScO_3$ [179]

strain, tensile strain induced an upshift of the O 2*p*-band center in relation to the Fermi level [176]. The O 2*p*-band center thus establishes a relationship between effects of strain and a variety of physical and chemical characteristics. In addition to electrical factors like work function, the position of the O 2*p*-band center relative to the Fermi level is also related to bulk oxygen vacancy formation energy in lanthanide perovskites (Fig. 10b) [177]. Because of the strain's impacts on the d-band and O 2*p*-band centers and variations in metal–oxygen overlap, strain affects surface properties like oxygen dissociative adsorption energy. Therefore, strain regulation can affect the oxygenated species during the electrocatalysis, which improves the rate-determining step of oxygen electrocatalysis (e.g., HOO*→O* in acidic OER). Theory indicates that under highly strained conditions, tensile strain can diminish the dissociation of surface oxygen relative to bulk for early transition metals (Sc-Co), while having the reverse effect for later transition metals (Ni-Cu) (Fig. 10c) [175]. As a result, strain has an influence on electrocatalysis performance, with compressively stretched $LaNiO_3$ catalysts displaying increased OER/ORR activity (Fig. 10d) [110]. Recently, it has been reported that spintronic and ferroelectric polarization regulation enhances the oxygen evolution efficiency of multiferroic oxides [178]. Thus, strain effects on ferroelectric polarization are also a promising method to adjust the oxygen electrocatalysis. As expected, the cumulative effects of strain result in a significant increase in ferroelectricity in strained $BaTiO_3$ relative to the unstrained state (Fig. 10e) [179].

Oxygen vacancy formation ($\Delta H_{vacancy\ formation}$) and migration energetics ($\Delta H_{vacancy\ migration}$) may be altered by strain, which is important for altering oxygen vacancy transport [180], oxygen surface exchange rate [181], and oxygen vacancy ordering [182]. The oxygen vacancy formation energy is reduced by moving the bulk O 2*p*-band center closer to the Fermi level, which improves the favorability of oxygen vacancy formation (Fig. 10b). The ease of electron transport from (to) oxygen states at the Fermi level upon oxygen addition (removal) and its connection with the weak metal–oxygen bond strength in bulk are the causes for this drop in vacancy formation energy [183]. Strain modifies the formation energy of oxygen vacancies in comparison with the unstrained bulk state via altering the O 2*p*-band center. By means of this strain-defect connection, the structural effects of strain are linked to the chemical ionic properties of perovskite oxides. These impacts from strain on oxygen

vacancy and interstitial formation energies of perovskite oxides might affect the oxygen interstitial dissuasion, especially in Ruddlesden-Popper oxide family [184, 185]. The barriers to oxygen migration, which are frequently mediated by vacancies in perovskites, are also altered by strain. In $La_{2-x}Sr_xNiO_4$, tensile strain has been found to reduce the barriers to interstitial migration of both oxide and peroxide interstitial species (Fig. 11a) [184]. Meyer et al. discovered that oxygen nonstoichiometry in strained cuprates is mediated by strain-modified surface exchange kinetics. Tensile-strained $La_{1.85}Sr_{0.15}CuO_4$ (LSCO) exhibits an oxygen exchange rate that is about one order of magnitude faster than a compressively strained film (Fig. 11b). The reduced oxygen interstitial migration barrier can also be applied for oxygen transport in membranes. In these membranes, oxygen transport requires the coordination of several different processes, including membrane surface reactions for oxygen exchange from the molecular state to lattice oxygen and vice versa (oxygen reduction and evolution), as well as concurrent oxygen ionic and electronic conduction. For instance, $Pr_2Ni_{1-x}Mo_xO_4$ displays excellent oxygen transport performance due to a high interstitial oxygen mobility, with significantly reduced diffusion barrier of oxygen (Fig. 11c) [186]. Moreover, the adsorption energy of oxygen and oxygenated adsorbates (*OH, *OOH) on $LaBO_3$ perovskites have been observed to change linearly with the O 2*p*-band center, making it an excellent electronic structural descriptor for surface reactivity during OER (Fig. 11d), and ORR (Fig. 11e) [187, 188]. The adsorption free energy of OER/ORR reaction intermediates at the bare surfaces may be used to generate theoretical OER/ORR volcano plots when the surfaces exhibit little coverage dependence. Both the ORR and OER activity volcano plots may be represented in the same volcano map by following the four OER/ORR charge transferring phases and making use of the scaling connections between surface reaction free energies and a surface binding energy descriptor. G(O*)-G(HO*) was used as the OER activity descriptor for the hypothetical OER activity volcano plot, and G(HO*) was used as the ORR activity descriptor for the hypothetical ORR activity volcano plot in order to more clearly show the trend (Fig. 11f) [188]. Because of the influence of strain on both bulk and surface energetics stated above, the capacity to controllably modify electrical and chemical properties has a substantial impact on not only room-temperature oxygen electrocatalysis but also high-temperature oxygen electrocatalysis.
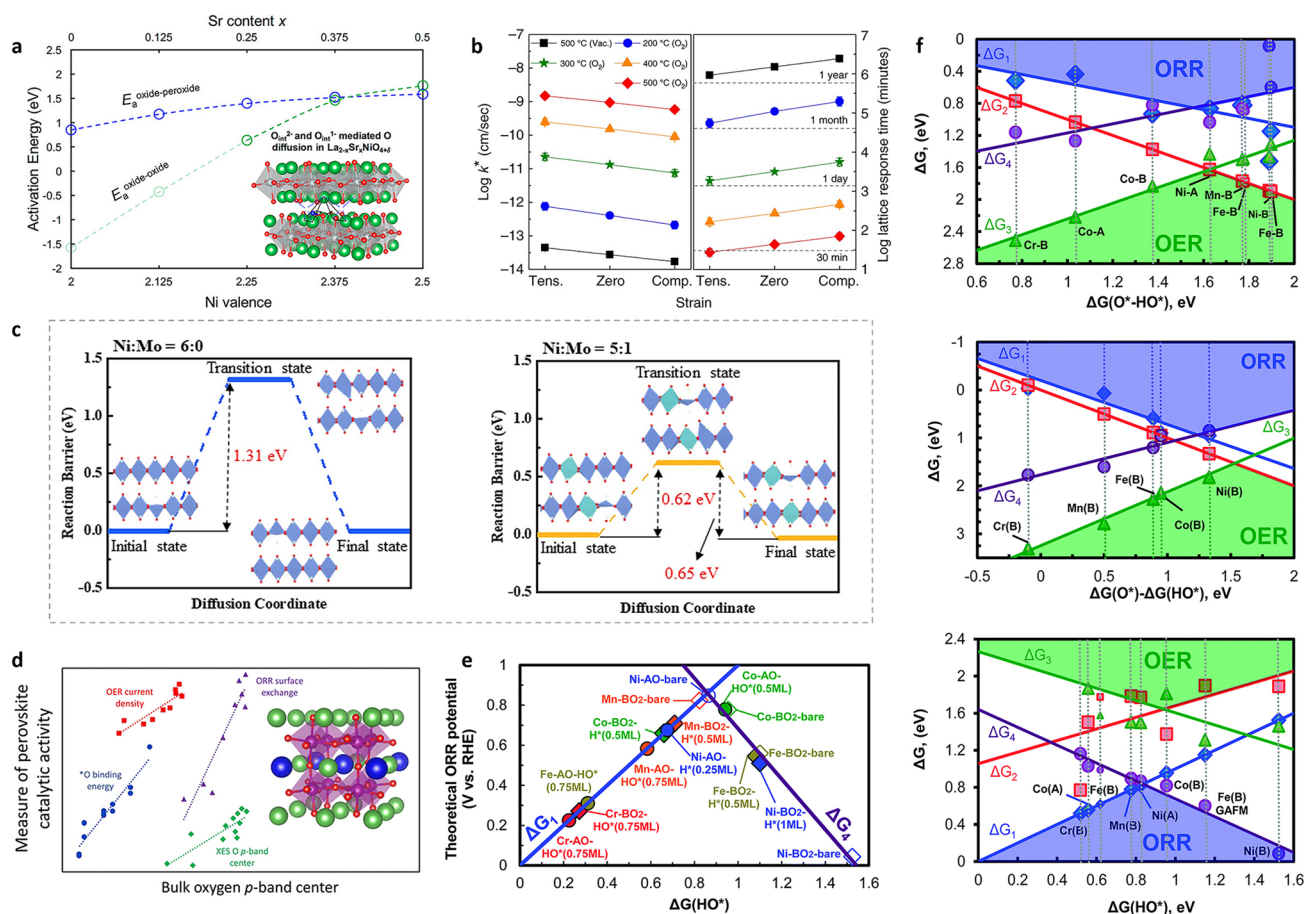
Fig. 11 **a** Activation energies of the oxide–oxide and oxide–peroxide diffusion mechanisms [184]. **b** Strain-dependent oxygen kinetics of $La_{1.85}Sr_{0.15}CuO_4$. Variation of predicted oxygen surface exchange rate k* and time required to incorporate oxygen under different annealing conditions and strain states [185]. **c** Diffusion pathway (insets) and the corresponding diffusion barrier of oxygen in the lattice of Pr_2NiO_4 and $Pr_2Ni_{5/6}Mo_{1/6}O_4$ [186]. **d** Correlations of perovskite catalytic performance with oxygen p-band bulk descriptor [187]. **e** Theoretical ORR volcano plot. **f** Calculated ΔG_1 ($H_2O(l)+* \rightarrow HO^*+H^+ +e^-$), ΔG_2 ($HO^* \rightarrow O^*+H^+ +e^-$), ΔG_3 ($O^*+H_2O(l) \rightarrow HOO^*+H^+ +e^-$), and ΔG_4 ($HOO^* \rightarrow O_2(g)+H^+ +e^-$) *vs.* $\Delta G(O^*-HO^*)$ [188]

The kind of proton–electron transfer that occurs during elementary reaction steps can be altered by the manipulation of electronic structure via strain effects [172]. The formation of thin films of $Ba_{0.5}Sr_{0.5}Co_{0.8}Fe_{0.2}O_{3-\delta}$ on $La_{0.8}Sr_{0.2}MnO_{3-\delta}$ improves the OER/ORR performance (Fig. 12a) [189]. Petrie et al. stretched the conducting perovskite $LaNiO_3$ epitaxially to investigate its effect on ORR/OER (Fig. 12b) [110]. This work indicated that compressive strain considerably improves both processes, resulting in a bifunctional catalyst that outperforms precious metals. The enhanced bifunctionality is attributed to strain-induced splitting of the e_g orbitals, filling of the out-of-plane d_{z2} orbitals and altering the perovskite BO_6 octahedral, modifying orbital asymmetry at the surface [110]. The addition of tensile strain to catalysts (e.g.,

cobaltites and nickelates) to increase oxygen vacancy formation has shown to be beneficial for the construction of higher activity catalysts. When a small biaxial tensile strain (2%) is applied to $SrCoO_3$ films, the favorability for oxygen vacancy formation (with a 30% decrease in oxygen activation energy barrier) manifests itself as a minor increase in Co^{3+} and a decrease in Co^{4+} species (Fig. 12c) [190]. These results are further supported by the anodic oxidation studies of $SrCoO_3$ films, where the film with the highest tensile-stress displayed a larger anodic potential for oxygen intercalation (Fig. 12d) as a result of increased tensile strain and a higher activity for OER (Fig. 12e) after the vacancy filling via oxygen intercalation [191]. The fact that tensile strain promotes the oxygen exchange kinetics and even oxygen transport was
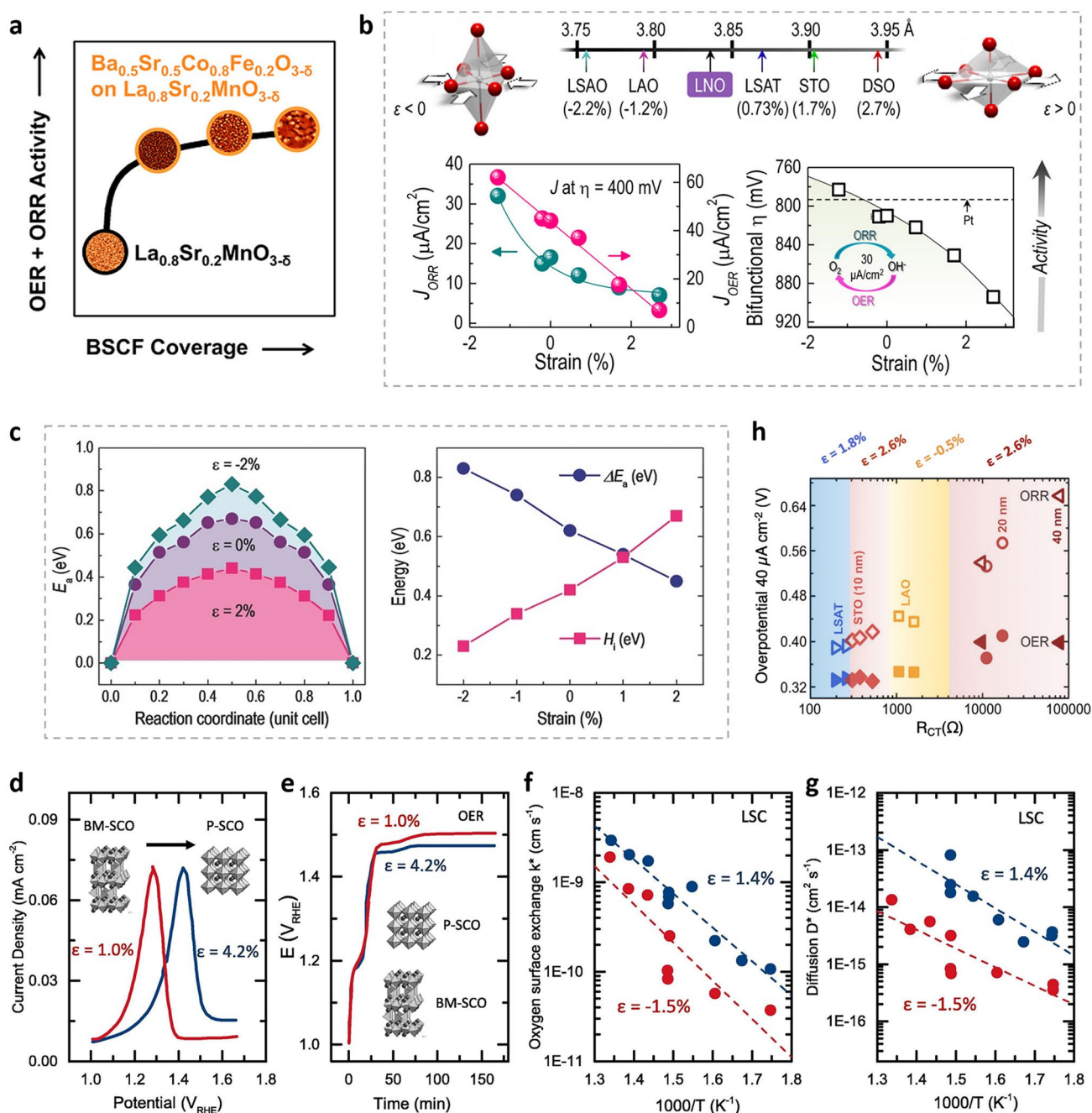
Fig. 12 **a** Bifunctional composite catalyst for oxygen electrocatalysis (ORR and OER) [189]. **b** Enhanced ORR and OER bifunctional activities using compressive strain [110]. **c** Strain-dependent oxygen activation [190]. **d** Anodic scan around the topotactic transformation peak as brownmillerite $SrCoO_{2.5}$ (BM-SCO) is oxidized to the perovskite $SrCoO_3$ (P-SCO) at 10 mV s^{-1} scan rate [191]. **e** Galvanostatic stability scans at 5 μA under different tensile strains in O2-saturated 0.1 M KOH [191]. **f** k* and **g** D* coefficients as a function of temperature for $La_{0.8}Sr_{0.2}CoO_{3-\delta}$ (LSC) [181]. **h** The overpotential of OER (filled) and ORR (open) on LCO corresponds with the charge transfer resistance, R_{CT}, measured at open circuit under different tensile strains ($\varepsilon = 1.8\%$, 2.6%, and -0.5%) [111]

also observed in $La_{0.8}Sr_{0.2}CoO_{3-\delta}$ (LSC) (Fig. 12f, g) [181]. Additionally, strain can change the rate at which charges move across the interface between electrode and electrolyte.

It is the origin of enhanced charge transfer process that led to higher OER catalytic current or lower overpotential for the OER/ORR happing. Meanwhile, strain is not a single

isolated factor; the strain changes are always along with the lattice changes of crystal. Then, the metal–oxygen bond length, in another word, the covalent between metal and oxygen would also be adjusted. The adjusted oxidation state of metal sites would lead to modulated charge transfer rate and even catalytic activity. Thus, strain would affect the OER/ORR performance via affect the charge transfer rate. As shown in Fig. 12h, according to substrate-induced and film thickness-induced stresses in $LaCoO_3$, moderately tensile-strained $LaCoO_3$ thin films grown on LSAT (1.8% strain), grown on STO (2.6% strain), and finally compressively strained films grown on LAO (−0.5% strain), demonstrated the highest OER and ORR activity (LCO) [111]. To date, a great deal of research has been done on strain engineering to help with the design of oxygen electrocatalysts. However, it should be noted that properly characterizing and modulating the strain effect remains a very difficult task.

4 Oxygen Electrocatalysis Related Applications

Exploration of high-performance energy conversion and storage (ECS) technologies such as regenerative fuel cells, metal–air batteries, and small molecule (N_2, CO_2, H_2O) electrolyzers capable of harvesting, converting, and storing renewable energy in chemicals and then reconverting at the point of need is critical, but it remains a scientific challenge [192]. Because it supplies electrons in electrochemical reactions that convert (renewable) electrical energy and chemical fuels, the OER and/or ORR module is a critical component in modern ECS systems. Firstly, the OER happens at the anode of an electrolyzer used to generate chemical fuel by electrolysis of water molecules (Fig. 13a) [193]. For example, water splitting: oxygen electrocatalysts can also be used in water splitting applications, where water is split into oxygen and hydrogen [129, 194–196]. This process is used in the production of hydrogen fuel for use in fuel cells. Secondly, oxygen electrocatalysis is also used in metal–air batteries, where oxygen is the cathode reactant. Metal–air batteries have a high energy density and are being developed as a promising alternative to traditional lithium-ion batteries. In which the ORR occurs on the positive electrode in metal–air batteries depicted in Fig. 13b [193], its activity and stability impact the charging and discharging performances of metal–air batteries [130, 197, 198]. Among various oxide

catalysts, the perovskite catalysts display excellent performance as bifunctional OER/ORR catalysts with potential for Zn-air battery (Table 3). Thirdly, oxygen electrocatalysis is a crucial aspect of fuel cell technology. In a fuel cell, oxygen is reduced at the cathode, producing water and generating electricity. A regenerative fuel cell, which functions in two modes of hydrogen production (electrolyzer cell mode) and power production (fuel cell mode), can only provide efficient long-term energy storage and on-demand conversion back to electrical energy through oxygen electrocatalysts (Fig. 13c) [193]. Oxygen electrocatalysts play a critical role in facilitating this process, improving the efficiency and performance of fuel cells. Acidic OER is more applicable compared to alkaline OER to commercialization because of the successful development and large-scale applications of proton exchange membranes (PEM), which have high proton conductivity, high voltage efficiency, low Ohmic loss, high current density, and high gas purity [55, 199]. More significant, an inherent advantage of acidic electrolytes over alkaline electrolytes is that hydronium ions have a far greater conductivity (350 S cm^2 mol^{-1}) than hydroxide ions (198 S cm^2 mol^{-1}). Thus, three energy conversion electrolyzers using PEM technology are shown in Fig. 13d, such as water electrolysis, nitrogen reduction and CO_2 reduction. Meanwhile, ORR is mainly connected to metal–air batteries (Fig. 13b) [200] and regenerative fuel cells (Fig. 13d) [103]. Overall, oxygen electrocatalysis is a key area of research with numerous applications in clean energy production, environmental remediation and chemical synthesis.

Oxygen electrocatalysis (OER and ORR) in solution is closely related to OER and ORR in solid oxide fuel cells (SOFC) and solid oxide electrolysis cells (SOEC). In addition to the oxygen electrocatalysis in aqueous system, oxide catalysts are also widely applied in SOFC and SOEC [214, 215]. There is a close relationship between OER and ORR, and SOFC and SOEC. These four processes all involve the electrochemical reactions of oxygen molecules. SOFC and SOEC are efficient energy conversion and storage systems that enable high-efficiency energy conversion, including electrochemical reactions where OER and ORR are important reactions [216, 217]. SOFC reacts hydrogen (or other fuels) and oxygen to produce electricity, water, and heat, where oxygen is reduced to oxygen ions. On the other hand, SOEC drives the electrochemical reduction of oxygen molecules to produce hydrogen or other combustible gases using electricity. Therefore, SOFC and SOEC are essentially
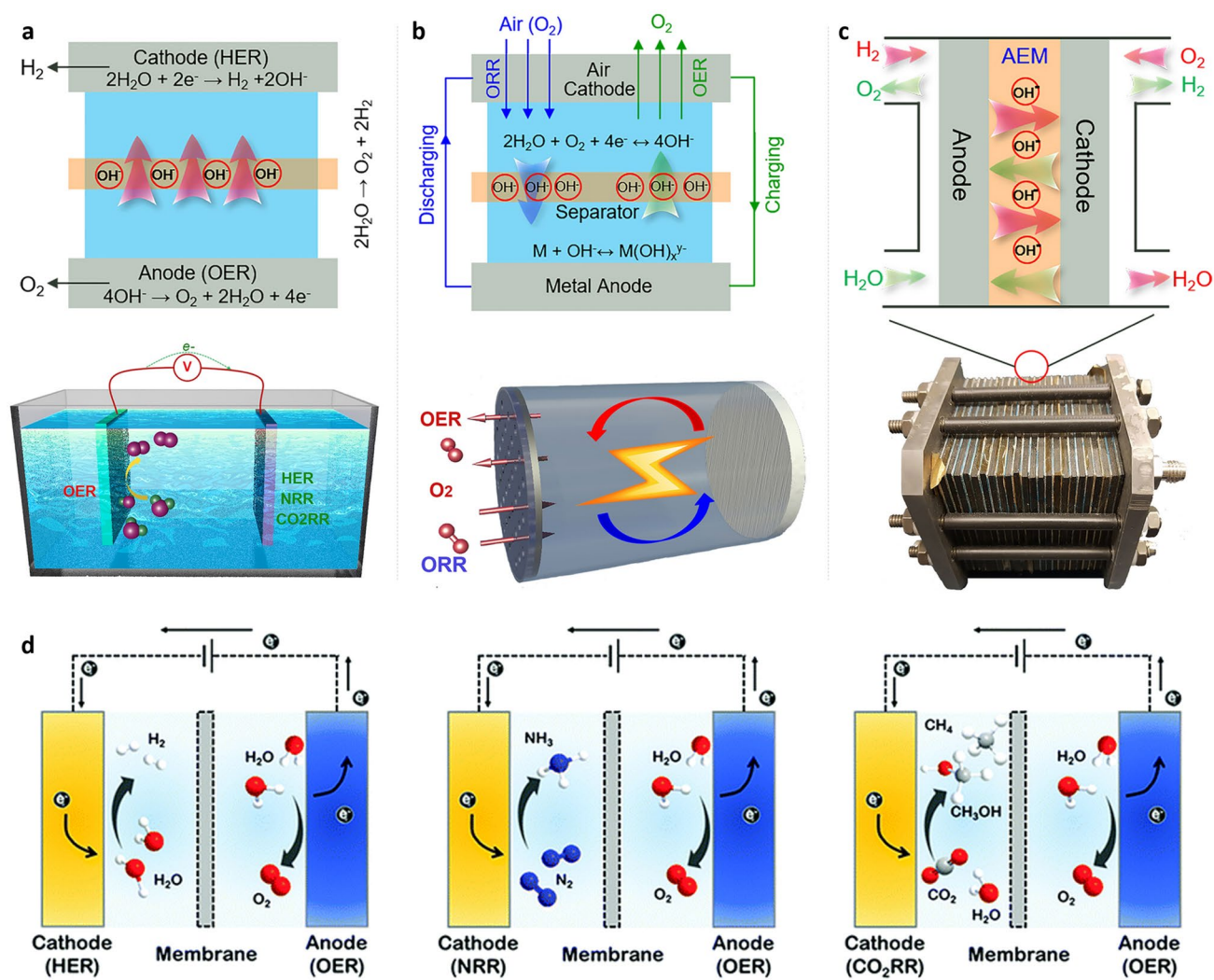
Fig. 13 OER in electrochemical energy conversion and storage devices. **a** Electrolyzers for small molecules' electrolysis. **b** Metal–air batteries. **c** Regenerative fuel cells [193]. **d** Scheme of several energy conversion electrolyzers relying on PEM: water electrolysis, nitrogen reduction and CO_2 reduction

the reverse processes of OER and ORR. In these processes, the activation energy of oxygen molecules can be adjusted by increasing the temperature or applying a voltage. By raising the temperature or applying a voltage, the energy of oxygen molecules will increase, which will help to reduce the activation energy of OER and ORR reactions, thereby improving reaction rates and efficiency. In addition, solid oxide materials serving as catalysts can also affect the rate and efficiency of OER and ORR reactions by adjusting their surface structures and electronic properties.

A SOFC is an electrochemical device that can either generate electricity with high efficiency or operate in reverse mode (as electrolyzer, SOEC) to produce chemical compounds (fuels) from electricity (Fig. 14a, b). SOFC is a potential technology for assisting in decarbonization and the development of sustainable energy systems. The key benefits of this technology are the following. (1) Fuel Flexibility: as a SOFC may use hydrocarbon fuel as well as varied compositions of biofuel and hydrogen derived from renewable sources, this is essential to the zero-emission transition. (2) Efficiency: the performance of SOFC fuel cells is significantly higher than that of internal combustion and coal-fired engines. According to the 2019 Fuel Cell Industry Review, commercial SOFC electricity generators now have an efficiency of 55% to 60% to more than 80% when utilized in Combined Heat Power systems (CHP). (3) Water generation:

Table 3 Summary of OER and ORR bifunctional oxygen perovskite electrocatalysts in 0.1 M KOH solution

| Catalyst	E_{onset} ORR	E_{onset} OER	Tafel slope OER (mV dec^{-1})	Tafel slope ORR (mV dec^{-1})	Refs
$La_{0.8}Sr_{0.2}MnO_3$	-0.2 V vs, Ag/AgCl	0.60 V vs. Ag/AgCl			[201]
$LaNi_{0.85}Mg_{0.15}O_3$		0.82	95	105	[202]
$La_{0.9}Sr_{0.1}CoO_3$	0.806 V vs. RHE	1.612 V vs. RHE			[203]
$Ba_{0.9}Co_{0.5}Fe_{0.4}Nb_{0.1}O_{3-\delta}$	-0.2 V vs, Ag/AgCl	0.59 V vs. Ag/AgCl			[204]
$BaMnO_3$	-0.19 V vs. Ag/AgCl	0.60 V vs. Ag/AgCl			[205]
$LaCo_{0.8}Mn_{0.2}O_3$	-0.21 V vs. Ag/AgCl	0.64 V vs. Ag/AgCl			[206]
$Ba_{0.5}Sr_{0.5}Co_{0.8}Fe_{0.2}O_3$	-0.18 V vs. Ag/AgCl	0.50 V vs. Ag/AgCl			[207]
$BaTiO_3$	0.88 V vs. RHE	1.3 V vs. RHE			[208]
$LaMnO_3$	0.78 V vs. RHE	154 mV dec^{-1}		110.2 mV dec^{-1}	[202]
$(La_{0.8}Sr_{0.2})_{0.95}Mn_{0.95}Ir_{0.05}O_3$	-0.05 V vs. Ag/AgCl	0.48 V vs. Ag/AgCl	103 mV dec^{-1}		[209]
$(La_{0.8}Sr_{0.2})_{0.9}Mn_{0.9}Co_{0.1}O_3$	-0.09 V vs. Ag/AgCl	0.67 V vs. Ag/AgCl			[210]
$LaCo_{0.5}Ni_{0.5}O_3$			73.9 mV dec^{-1}	112 mV dec^{-1}	[211]
$La_{0.95}FeO_3$	0.58 vs RHE	1.64 vs. RHE			[148]
$La_{0.6}Sr_{0.4}CoO_{3-\delta}$	-0.187 vs Hg/HgO	0.893 vs. Hg/HgO			[212]
$La_{0.5}Sr_{0.5}CoO_{2.91}$	0.78 vs RHE	1.84 vs. RHE			[213]
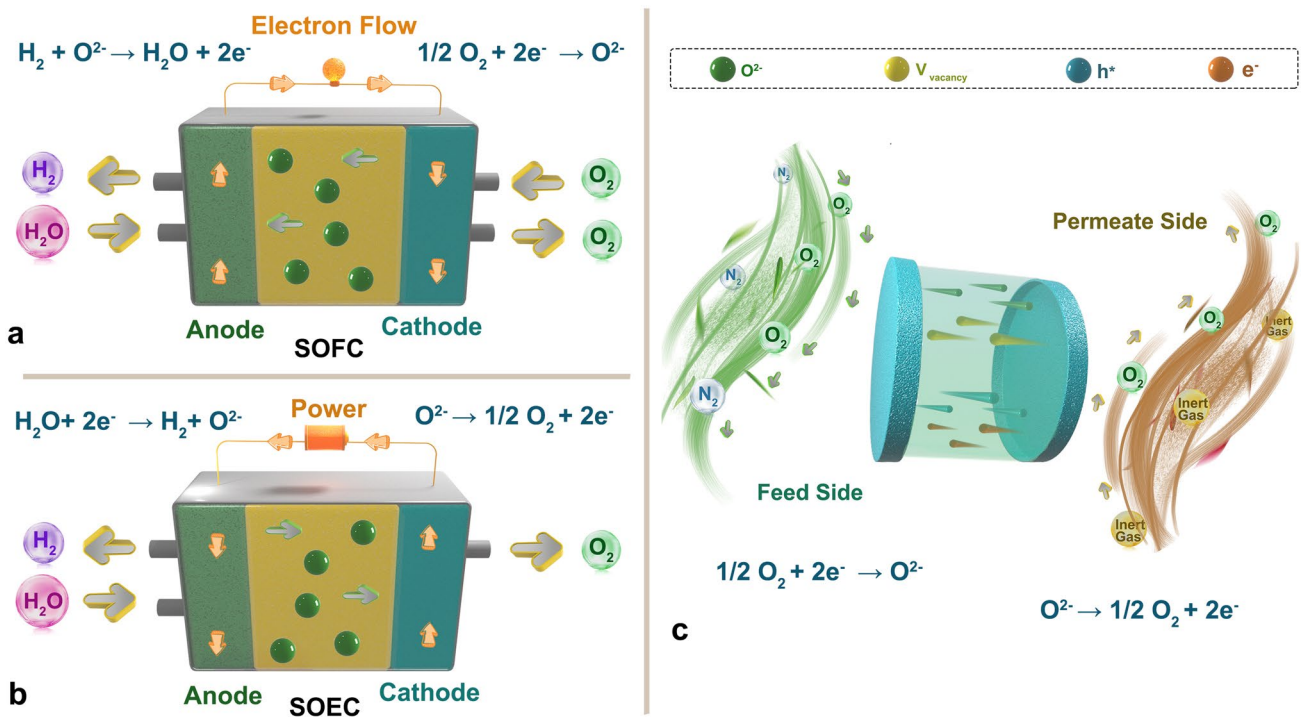
Fig. 14 Schematic of working principle of **a** SOFC and **b** SOEC. **c** Schematic of working principle of MIEC materials-based oxygen separation membrane

SOFC generates water as a by-product of power generation, an obvious advantage over traditional energy sources. Fuel cell utilization in the energy industry has the potential to minimize water use and withdrawals. (4) Scalability: this is an imperative feature that may be provided by employing a distributed energy generator since the initial installation and operation do not necessitate significant capital expenditures and it can be expanded as demand increases. This is

feasible because more fuel cell modules may be added in parallel to improve the power output. (5) Low carbon emission: SOFCs are regarded near-zero emission devices due to their operating principle. Furthermore, if the fuel is pure hydrogen, SOFC products are nothing more than water and heat. (6) Materials: the layers of the SOFC are constructed of ceramic, which eliminates the use of precious metal as catalytic material, making the device much cheaper.

To achieve good SOFC performance, the catalysts at the anode and the cathode are very important, while the electrolyte should have low electronic conductivity but high oxygen mobility [218–220]. At the anode, fuels such as H_2 and natural gas are oxidized. Due to the high temperature inside the cell, anodic materials need to have high electrical conductivity, high stability, thermal compatibility with other cell components, electrocatalytic activity for oxidation reactions, and porosity for effective transport of carrier gases in a reducing atmosphere. Pure porous metallic electrodes, such as Ni, Pt and Ru, have been utilized as anodes [221]. A lot of perovskite-like oxides such as $Ba_{0.5}La_{0.5}Ti_{0.3}Mn_{0.7}O_3$, $Ba_{0.5}La_{0.5}In_{0.3}Ti_{0.1}Mn_{0.6}O_3$ [222], and $La_{1-x}Sr_xMnO_3$ [223] were also investigated as anode catalyst for SOFC. The reduction of oxygen to O^{2-} ions on the surface into lattice vacancies is required for catalysts at cathode. Oxides such as cobalt perovskites ($LaCoO_3$, $SrCoO_3$, and $La_{1-x}Sr_xCoO_{3-\delta}$), iron-contained perovskites ($SrFeO_3$ and $La_{1-x}Sr_xFeO_{3-\delta}$), and Ni/Cu-layered perovskite-like oxides [224–227] with good mixed oxygen ionic and electronic conductivity (MIEC) are widely applied as cathode in SOFC [228].

In SOFC, OER and ORR occur at the cathode and anode, respectively, driving the fuel cell reaction to generate electricity. In SOEC, OER and ORR also occur at the anode and cathode, enabling water splitting and hydrogen production through reverse current. However, the solid oxide electrolyte used in SOFC and SOEC requires high temperature to operate, which poses many technical challenges in practical applications, such as thermal stability and mechanical strength. In contrast, water-based OER and ORR typically occur at lower temperatures, making them more suitable for low-temperature energy conversion and storage applications. By studying the catalytic mechanism and catalyst design of OER and ORR, more efficient and stable catalysts can be provided for solid SOFC and SOEC, enabling more sustainable energy conversion and storage. Moreover, based on the intrinsic oxygen reduction property as cathode in SOFC and oxygen evolution property as anode in SOEC

with, these catalysts are also widely investigated directly as oxygen transport membrane [229, 230]. Oxygen has been recognized as an essential chemical for power plants based on fossil fuel consumptions such as integrated gasification combined cycle and oxy-fuel combustion, which have been recognized as the most realistic clean energy technologies for energy production with carbon capture and storage. Unfortunately, most of the current industrial oxygen production is achieved by pressure swing adsorption and the cryogenic distillation process. These conventional methods are costly and energy-intensive, releasing substantial amounts of CO_2 release. Dense ceramic membranes made from MIEC materials have attracted interest due to their advantages such as high selectivity (nearly 100% for oxygen) and energy- and cost-efficiency [231–233]. Among the MIEC materials studied, perovskite oxides are the focus of research due to their high oxygen permeation flux rates [186, 234–236] For such kinds of membranes, the oxygen transport requires a good match of multiple functions: membrane surface reactions for oxygen exchange from the molecular state to lattice oxygen (oxygen reduction) and vice versa (oxygen evolution); and the concomitant ionic oxygen and electronic conduction (Fig. 14c) [237].

5 Conclusion and Outlook

In conclusion, the rational design of oxide catalysts for oxygen electrocatalysis has the potential to revolutionize various fields, from clean energy production to and chemical synthesis. By understanding the fundamental principles underlying the catalytic activity of oxides, researchers can design new catalysts with enhanced performance and durability [238–241]. To designing oxide catalysts is to manipulate their electronic and geometric structures. This can be achieved through the use of element doping, defecting engineering, among other techniques. These modifications can enhance the catalytic activity of oxides by creating active sites, increasing the surface area, and optimizing the electronic properties of the catalyst. Moreover, to explore new oxide materials with unique properties, such as perovskites, spinels, and layered double hydroxides. These materials offer advantages such as high conductivity, high surface area, and structural diversity, which can be leveraged to enhance the catalytic activity of the oxide. OER and ORR have attracted considerable attention due to their potential use in various

energy conversion and storage systems, including water electrolyzers, metal–air batteries, electrochemical energy conversion and storage systems. However, despite significant progress made in the design of oxide catalysts for OER and ORR, there are still several challenges that need to be addressed to enable their widespread use.

(a) To improve the catalytic activity of oxide catalysts towards ORR or OER. Although many oxide catalysts have been reported to exhibit good ORR or OER activity, their performance still falls short of that of precious metal-based catalysts. This is partly due to the sluggish kinetics and complex reaction mechanisms of ORR or OER, which require highly active and selective catalysts. Therefore, there is a need for further research into the fundamental mechanisms underlying the ORR or OER process, and how they can be tailored to enhance the activity of oxide catalysts.

(b) To improve the stability of oxide catalysts under the harsh operating conditions of electrochemical devices. Many oxide catalysts are prone to degradation and deactivation due to the corrosive nature of the electrolyte, high temperature, and high pressure. Moreover, the formation of oxide layers and surface defects can also lead to the loss of catalytic activity over time. Therefore, there is a need for the development of new synthesis and processing methods to improve the stability and durability of oxide catalysts under such conditions.

(c) To improve the scalability and cost-effectiveness of the synthesis of oxide catalysts. Most oxide catalysts are synthesized through high-temperature solid-state reactions or sol–gel methods, which are often time-consuming, energy-intensive, and difficult to scale up. Therefore, there is a need for the development of new synthesis methods that can produce oxide catalysts at low cost and in large quantities, while maintaining their high activity and stability.

(d) To deeply explore the reaction mechanism of oxide catalysts during oxygen electrocatalysis. Investigate the real active sites/centers and the mechanism, isotope tracing experiments should be conducted. For example, the oxide catalysts for OER will happen via two different reaction mechanisms: adsorbate evolution mechanism (AEM) and lattice oxygen-mediated mechanism or lattice oxygen oxidation mechanism (LOM). The real reaction process/mechanism of the synthesized catalyst could be investigated via ^{18}O isotope detection of the reaction product as well as density functional theory calculations. It will directly detect the participation of oxygen anions from the oxide lattice as an active intermediary in the OER.

(e) To explore the intermediates will give rise to the understanding of the reaction process/step and the real mechanism. Thus, it is suggested to further explore the intermediates combined with the isotope tracing experiments, theoretical calculations, and direct proof via in situ characterizations. For example, in situ attenuated total reflection surface-enhanced infrared absorption spectroscopy (ATR-SEIRAS) measurement was highly sensitive to oxygen-containing intermediates, which could be introduced into OER and ORR investigation. More in situ characterization experiments should be conducted for the deep understanding of the real relationship between catalysts and catalytic performance (stability and activity) from phase structure to oxidation state. The in situ X-ray absorption spectroscopy (XAS) measurement could be introduced as in situ X-ray absorption near edge structure (XANES) is useful for in situ oxidation state exploration. The in situ extended X-ray absorption fine structure (EXAFS) is useful for the in situ crystal exploration. This directly obtained information can help to understand the reaction mechanisms and thus guide the design of promising catalysts.

Oxide catalysts hold great promise for use in electrochemical energy conversion and storage systems, but there are significant challenges that need to be addressed in their development for oxygen reduction and oxygen evolution reactions. Improving their catalytic activity, stability, and scalability is crucial for their widespread adoption and for reducing our reliance on fossil fuels, while also mitigating the environmental impact of energy production. The rational design of oxide catalysts for oxygen electrocatalysis is critical for advancing the development of fuel cells, metal–air batteries, water splitting, and carbon capture technologies, which can significantly reduce greenhouse gas emissions, improve energy efficiency, and enhance the sustainability of our energy systems. Continued research in this area is of utmost importance for a cleaner and more sustainable future. By addressing the challenges associated with oxide catalysts for ORR and OER, we can make significant strides towards a cleaner and more sustainable future. The development of these catalysts has the potential to revolutionize the way we produce and store energy, ultimately making our energy systems more efficient and environmentally friendly. Therefore, continued investment in research in this area is

essential to unlock the full potential of oxide catalysts and their applications.

Declarations

Conflict of interest The authors declare no interest conflict. They have no known competing financial interests or personal relationships that could have appeared to influence the work reported in this paper.

References

1. C. Zhang, J. Sunarso, S. Liu, Designing CO_2-resistant oxygen-selective mixed ionic-electronic conducting membranes: Guidelines, recent advances, and forward directions. Chem. Soc. Rev. **46**(10), 2941–3005 (2017). https://doi.org/10.1039/c6cs00841k

2. W. Wang, C. Su, Y. Wu, R. Ran, Z. Shao, Progress in solid oxide fuel cells with Nickel-based anodes operating on methane and related fuels. Chem. Rev. **113**(10), 8104–8151 (2013). https://doi.org/10.1021/cr300491e

3. N. Han, X. Guo, J. Cheng, P. Liu, S. Zhang et al., Inhibiting in situ phase transition in Ruddlesden-popper perovskite via tailoring bond hybridization and its application in oxygen permeation. Matter **4**, 1720–1734 (2021). https://doi.org/10.1016/j.matt.2021.02.019

4. A. Kumar, A. Kumar, V. Krishnan, Perovskite oxide based materials for energy and environment-oriented photocatalysis. ACS Catal. **10**(17), 10253–10315 (2020). https://doi.org/10.1021/acscatal.0c02947

5. R. Shi, Z. Wang, Y. Zhao, G.I.N. Waterhouse, Z. Li et al., Room-temperature electrochemical acetylene reduction to ethylene with high conversion and selectivity. Nat.

6. Z. Wang, X. Li, Z. Yang, H. Guo, Y.J. Tan et al., Fully transient stretchable fruit-based battery as safe and environmentally friendly power source for wearable electronics. EcoMat **3**(1), e12073 (2021). https://doi.org/10.1002/eom2.12073

7. K. Liu, J. Lang, M. Yang, J. Xu, B. Sun et al., Molten lithium-brass/zinc chloride system as high-performance and low-cost battery. Matter **3**(5), 1714–1724 (2020). https://doi.org/10.1016/j.matt.2020.08.022

8. R. Razaq, P. Li, Y. Dong, Y. Li, Y. Mao et al., Practical energy densities, cost, and technical challenges for magnesium-sulfur batteries. EcoMat **2**(4), e12056 (2020). https://doi.org/10.1002/eom2.12056

9. K. Xie, N. Umezawa, N. Zhang, P. Reunchan, Y. Zhang et al., Self-doped $SrTiO_{3-\delta}$ photocatalyst with enhanced activity for artificial photosynthesis under visible light. Energ. Environ. Sci. **4**(10), 4211–4219 (2011). https://doi.org/10.1039/C1EE01594J

10. U.G.M. Ekanayake, D.H. Seo, K. Faershteyn, A.P. O'Mullane, H. Shon et al., Atmospheric-pressure plasma seawater desalination: clean energy, agriculture, and resource recovery nexus for a blue planet. Sustain. Mater. Technol. **25**, e00181 (2020). https://doi.org/10.1016/j.susmat.2020.e00181

11. N. Han, P. Liu, J. Jiang, L. Ai, Z. Shao et al., Recent advances in nanostructured metal nitrides for water splitting. J. Mater. Chem. A **6**(41), 19912–19933 (2018). https://doi.org/10.1039/C8TA06529B

12. I. Concina, Z.H. Ibupoto, A. Vomiero, Semiconducting metal oxide nanostructures for water splitting and photovoltaics. Adv. Energy Mater. **7**(23), 1700706 (2017). https://doi.org/10.1002/aenm.201700706

13. H. Tian, J. Liang, J. Liu, Nanoengineering carbon spheres as nanoreactors for sustainable energy applications. Adv. Mater. **31**(50), 1903886 (2019). https://doi.org/10.1002/adma.201903886

14. J.D. Benck, T.R. Hellstern, J. Kibsgaard, P. Chakthranont, T.F. Jaramillo, Catalyzing the hydrogen evolution reaction (HER) with molybdenum sulfide nanomaterials. ACS Catal. **4**(11), 3957–3971 (2014). https://doi.org/10.1021/cs500923c

15. Y.P. Zhu, T.Y. Ma, M. Jaroniec, S.Z. Qiao, Self-templating synthesis of hollow Co_3O_4 microtube arrays for highly efficient water electrolysis. Angew. Chem. Int. Ed. **56**(5), 1324–1328 (2017). https://doi.org/10.1002/anie.201610413

16. J. Sun, X. Liu, S. Yang, "Highway" toward efficient water oxidation. Matter **4**(1), 21–22 (2021). https://doi.org/10.1016/j.matt.2020.12.010

17. S. Liu, J. Huang, H. Su, G. Tang, Q. Liu et al., Multiphase phosphide cocatalyst for boosting efficient photocatalytic H_2 production and enhancing the stability. Ceram. Int. **47**(1), 1414–1420 (2021). https://doi.org/10.1016/j.ceramint.2020.08.265

18. H. Lyu, T. Hisatomi, Y. Goto, M. Yoshida, T. Higashi et al., An Al-doped $SrTiO_3$ photocatalyst maintaining sunlight-driven overall water splitting activity for over 1000 h of

constant illumination. Chem. Sci. **10**(11), 3196–3201 (2019). https://doi.org/10.1039/C8SC05757E

19. W. Wang, M.O. Tadé, Z. Shao, Research progress of perovskite materials in photocatalysis- and photovoltaics-related energy conversion and environmental treatment. Chem. Soc. Rev. **44**(15), 5371–5408 (2015). https://doi.org/10.1039/C5CS00113G

20. P. Zhang, J. Zhang, J. Gong, Tantalum-based semiconductors for solar water splitting. Chem. Soc. Rev. **43**(13), 4395–4422 (2014). https://doi.org/10.1039/C3CS60438A

21. Y. Liu, W. Zeng, Y. Ma, R. Dong, P. Tan et al., Oxygen-defects modified amorphous Ta_2O_5 nanoparticles for solar driven hydrogen evolution. Ceram. Int. **47**(4), 4702–4706 (2021). https://doi.org/10.1016/j.ceramint.2020.10.038

22. H.G. Kim, D.W. Hwang, J. Kim, Y.G. Kim, J.S. Lee, Highly donor-doped (110) layered perovskite materials as novel photocatalysts for overall water splitting. Chem. Commun. **12**, 1077–1078 (1999). https://doi.org/10.1039/A902892G

23. M.G. Walter, E.L. Warren, J.R. McKone, S.W. Boettcher, Q. Mi et al., Solar water splitting cells. Chem. Rev. **110**(11), 6446–6473 (2010). https://doi.org/10.1021/cr1002326

24. J. Huo, Y. Chen, Y. Liu, J. Guo, L. Lu et al., Bifunctional Iron Nickel phosphide nanocatalysts supported on porous carbon for highly efficient overall water splitting. Sustain. Mater. Technol. **22**, e00117 (2019). https://doi.org/10.1016/j.susmat.2019.e00117

25. J. Hwang, R.R. Rao, L. Giordano, Y. Katayama, Y. Yu et al., Perovskites in catalysis and electrocatalysis. Science **358**(6364), 751–756 (2017). https://doi.org/10.1126/science.aam7092

26. J. Li, J. Li, J. Ren, H. Hong, D. Liu et al., Electric-field-treated Ni/Co_3O_4 film as high-performance bifunctional electrocatalysts for efficient overall water splitting. Nano-Micro Lett. **14**(1), 148 (2022). https://doi.org/10.1007/s40820-022-00889-3

27. Y. Liu, P. Vijayakumar, Q. Liu, T. Sakthivel, F. Chen et al., Shining light on anion-mixed nanocatalysts for efficient water electrolysis: fundamentals, progress, and perspectives. Nano-Micro Lett. **14**(1), 43 (2022). https://doi.org/10.1007/s40820-021-00785-2

28. H. Tian, A. Song, P. Zhang, K. Sun, J. Wang et al., High durability of Fe–N–C single-atom catalysts with carbon vacancies toward the oxygen reduction reaction in alkaline media. Adv. Mater. **35**(14), 2210714 (2023). https://doi.org/10.1002/adma.202210714

29. H. Tian, F. Huang, Y. Zhu, S. Liu, Y. Han et al., The development of yolk–shell-structured Pd&ZnO@Carbon submicroreactors with high selectivity and stability. Adv. Funct. Mater. **28**(32), 1801737 (2018). https://doi.org/10.1002/adfm.201801737

30. H. Tian, A. Song, H. Tian, J. Liu, G. Shao et al., Single-atom catalysts for high-energy rechargeable batteries. Chem. Sci. **12**(22), 7656–7676 (2021). https://doi.org/10.1039/D1SC00716E

31. Z. Ma, A. Song, Z. Liu, Y. Guo, X. Yang et al., Nanoconfined expansion behavior of hollow MnS@Carbon anode

with extended lithiation cyclic stability. Adv. Funct. Mater. (2023). https://doi.org/10.1002/adfm.202301112

32. L. Bai, A. Song, X. Lei, T. Zhang, S. Song et al., Hierarchical construction of hollow $NiCo_2S_4$ Nanotube@$NiCo_2S_4$ nanosheet arrays on ni foam as an efficient and durable electrocatalyst for hydrogen evolution reaction. Int. J. Hydrogen. Energ. **47**(91), 38524–38532 (2022). https://doi.org/10.1016/j.ijhydene.2022.09.020

33. H. Tian, H. Tian, S. Wang, S. Chen, F. Zhang et al., High-power lithium–selenium batteries enabled by atomic cobalt electrocatalyst in hollow carbon cathode. Nat. Commun. **11**(1), 5025 (2020). https://doi.org/10.1038/s41467-020-18820-y

34. H. Tian, X. Liu, L. Dong, X. Ren, H. Liu et al., Enhanced hydrogenation performance over hollow structured Co-CoOx@N-C capsules. Adv. Sci. **6**(22), 1900807 (2019). https://doi.org/10.1002/advs.201900807

35. J. Dai, Y. Zhu, Y. Yin, H.A. Tahini, D. Guan et al., Super-exchange interaction induced overall optimization in ferromagnetic perovskite oxides enables ultrafast water oxidation. Small **15**(39), 1903120 (2019). https://doi.org/10.1002/smll.201903120

36. Y. Yan, C. Liu, H. Jian, X. Cheng, T. Hu et al., Substitutionally dispersed high-oxidation CoO_x clusters in the lattice of rutile TiO_2 triggering efficient co-ti cooperative catalytic centers for oxygen evolution reactions. Adv. Funct. Mater. **31**(9), 2009610 (2021). https://doi.org/10.1002/adfm.202009610

37. Y. Zhao, X. Jia, G. Chen, L. Shang, G.I.N. Waterhouse et al., Ultrafine NiO nanosheets stabilized by TiO_2 from monolayer NiTi-LdH precursors: an active water oxidation electrocatalyst. J. Am. Chem. Soc. **138**(20), 6517–6524 (2016). https://doi.org/10.1021/jacs.6b01606

38. M. Luo, Z. Zhao, Y. Zhang, Y. Sun, Y. Xing et al., Pdo bimetallene for oxygen reduction catalysis. Nature **574**(7776), 81–85 (2019). https://doi.org/10.1038/s41586-019-1603-7

39. M. Luo, S. Guo, Strain-controlled electrocatalysis on multimetallic nanomaterials. Nat. Rev. Mater. **2**(11), 17059 (2017). https://doi.org/10.1038/natrevmats.2017.59

40. Q. Wang, N. Han, A. Bokhari, X. Li, Y. Cao et al., Insights into mxenes-based electrocatalysts for oxygen reduction. Energy **255**, 124465 (2022). https://doi.org/10.1016/j.energy.2022.124465

41. Y. Cao, W. Zhang, Y. Sun, Y. Jiang, N. Han et al., Highly active iron-nitrogen-boron-carbon bifunctional electrocatalytic platform for hydrogen peroxide sensing and oxygen reduction. Environ. Res. **201**, 111563 (2021). https://doi.org/10.1016/j.envres.2021.111563

42. Y. Cao, Y. Sun, N. Han, X. Li, Q. Wang et al., Novel highly active and selective consc efficient orr catalyst derived from In-SiTu egg gel pyrolysis. Fuel **333**, 126432 (2023). https://doi.org/10.1016/j.fuel.2022.126432

43. Y. Sun, W. Zhang, Q. Wang, N. Han, A. Núñez-Delgado et al., Biomass-derived N, S Co-doped 3d multichannel carbon supported Au@Pd@Pt catalysts for oxygen reduction.

Environ. Res. **202**, 111684 (2021). https://doi.org/10.1016/j.envres.2021.111684

44. Y. Cao, Y. Sun, R. Zheng, Q. Wang, X. Li et al., Biomass-derived carbon material as efficient electrocatalysts for the oxygen reduction reaction. Biomass. Bioenerg. **168**, 106676 (2023). https://doi.org/10.1016/j.biombioe.2022.106676

45. Z.-F. Huang, J. Song, S. Dou, X. Li, J. Wang et al., Strategies to break the scaling relation toward enhanced oxygen electrocatalysis. Matter **1**(6), 1494–1518 (2019). https://doi.org/10.1016/j.matt.2019.09.011

46. L. Yang, G. Yu, X. Ai, W. Yan, H. Duan et al., Efficient oxygen evolution electrocatalysis in acid by a perovskite with face-sharing IRO6 octahedral dimers. Nat. Commun. **9**(1), 5236 (2018). https://doi.org/10.1038/s41467-018-07678-w

47. Z. Chen, X. Gu, Y. Guo, X. Wang, M. Shao et al., A carbon dot-based total green and self-recoverable solid-state electrochemical cell fully utilizing O_2/H_2O redox couple. SusMat **1**(3), 448–457 (2021). https://doi.org/10.1002/sus2.23

48. W. Zhang, N. Han, J. Luo, X. Han, S. Feng et al., Critical role of phosphorus in hollow structures cobalt-based phosphides as bifunctional catalysts for water splitting. Small **18**(4), 2103561 (2022). https://doi.org/10.1002/smll.202103561

49. Y. Chen, J.K. Seo, Y. Sun, T.A. Wynn, M. Olguin et al., Enhanced oxygen evolution over dual corner-shared cobalt tetrahedra. Nat. Commun. **13**(1), 5510 (2022). https://doi.org/10.1038/s41467-022-33000-w

50. L. Li, P. Wang, Q. Shao, X. Huang, Recent progress in advanced electrocatalyst design for acidic oxygen evolution reaction. Adv. Mater. **33**(50), 2004243 (2021). https://doi.org/10.1002/adma.202004243

51. X. Wang, H. Zhong, S. Xi, W.S.V. Lee et al., Understanding of oxygen redox in oxygen evolution reaction. Adv. Mater. **34**(50), 2107956 (2021). https://doi.org/10.1002/adma.202107956

52. N. Zhang, C. Wang, J. Chen, Y. Chai, Oxygen reactivity regulation via double-exchange interaction for enhanced water oxidation. EcoMat **5**(2), e12290 (2022). https://doi.org/10.1002/eom2.12290

53. Y. Wen, C. Liu, R. Huang, H. Zhang, X. Li et al., Introducing brønsted acid sites to accelerate the bridging-oxygen-assisted deprotonation in acidic water oxidation. Nat. Commun. **13**(1), 4871 (2022). https://doi.org/10.1038/s41467-022-32581-w

54. Y. Zhang, X. Zhu, G. Zhang, P. Shi, A.-L. Wang, Rational catalyst design for oxygen evolution under acidic conditions: strategies toward enhanced electrocatalytic performance. J. Mater. Chem. A **9**(10), 5890–5914 (2021). https://doi.org/10.1039/D0TA11982B

55. X. Xu, H. Sun, S.P. Jiang, Z. Shao, Modulating metal–organic frameworks for catalyzing acidic oxygen evolution for proton exchange membrane water electrolysis. SusMat **1**(4), 460–481 (2021). https://doi.org/10.1002/sus2.34

56. Y. Pang, H. Xie, Y. Sun, M.-M. Titirici, G.-L. Chai, Electrochemical oxygen reduction for H_2O_2 production: catalysts, ph effects and mechanisms. J. Mater. Chem. A **8**(47), 24996–25016 (2020). https://doi.org/10.1039/D0TA09122G

57. A.T. Murray, S. Voskian, M. Schreier, T.A. Hatton, Y. Surendranath, Electrosynthesis of hydrogen peroxide by phase-transfer catalysis. Joule **3**(12), 2942–2954 (2019). https://doi.org/10.1016/j.joule.2019.09.019

58. O. Jung, M.L. Pegis, Z. Wang, G. Banerjee, C.T. Nemes et al., Highly active NiO photocathodes for H_2O_2 production enabled via outer-sphere electron transfer. J. Am. Chem. Soc. **140**(11), 4079–4084 (2018). https://doi.org/10.1021/jacs.8b00015

59. Y. Xia, X. Zhao, C. Xia, Z.-Y. Wu, P. Zhu et al., Highly active and selective oxygen reduction to H_2O_2 on boron-doped carbon for high production rates. Nat. Commun. **12**(1), 4225 (2021). https://doi.org/10.1038/s41467-021-24329-9

60. P. Morandi, V. Flaud, S. Tingry, D. Cornu, Y. Holade, Tartaric acid regulated the advanced synthesis of bismuth-based materials with tunable performance towards the electrocatalytic production of hydrogen peroxide. J. Mater. Chem. A **8**(36), 18840–18855 (2020). https://doi.org/10.1039/D0TA06466A

61. J. Yu, Q. He, G. Yang, W. Zhou, Z. Shao et al., Recent advances and prospective in ruthenium-based materials for electrochemical water splitting. ACS Catal. **9**(11), 9973–10011 (2019). https://doi.org/10.1021/acscatal.9b02457

62. H. Wang, Z.-N. Chen, D. Wu, M. Cao, F. Sun et al., Significantly enhanced overall water splitting performance by partial oxidation of ir through Au modification in core–shell alloy structure. J. Am. Chem. Soc. **143**(12), 4639–4645 (2021). https://doi.org/10.1021/jacs.0c12740

63. G. Zhang, Z.-A. Lan, L. Lin, S. Lin, X. Wang, Overall water splitting by Pt/g-C_3N_4 photocatalysts without using sacrificial agents. Chem. Sci. **7**(5), 3062–3066 (2016). https://doi.org/10.1039/C5SC04572J

64. C. Li, N. Clament Sagaya Selvam, J. Fang, Shape-controlled synthesis of Platinum-based nanocrystals and their electrocatalytic applications in fuel cells. Nano-Micro Lett. **15**(1), 83 (2023). https://doi.org/10.1007/s40820-023-01060-2

65. K. Kalantar-zadeh, J.Z. Ou, T. Daeneke, A. Mitchell, T. Sasaki et al., Two dimensional and layered transition metal oxides. Appl. Mater. Today **5**, 73–89 (2016). https://doi.org/10.1016/j.apmt.2016.09.012

66. V. Charles, A.O. Anumah, K.A. Adegoke, M.O. Adesina, I.P. Ebuka et al., Progress and challenges pertaining to the earthly-abundant electrocatalytic materials for oxygen evolution reaction. Sustain. Mater. Technol. **28**, e00252 (2021). https://doi.org/10.1016/j.susmat.2021.e00252

67. B. Guo, Y. Ding, H. Huo, X. Wen, X. Ren et al., Recent advances of transition metal basic salts for electrocatalytic oxygen evolution reaction and overall water electrolysis. Nano-Micro Lett. **15**(1), 57 (2023). https://doi.org/10.1007/s40820-023-01038-0

68. C. Wang, Q. Zhang, B. Yan, B. You, J. Zheng et al., Facet engineering of advanced electrocatalysts toward hydrogen/oxygen evolution reactions. Nano-Micro Lett. **15**(1), 52 (2023). https://doi.org/10.1007/s40820-023-01024-6

69. J. Suntivich, K.J. May, H.A. Gasteiger, J.B. Goodenough, Y. Shao-Horn, A perovskite oxide optimized for oxygen

evolution catalysis from molecular orbital principles. Science **334**, 1383–1385 (2011). https://doi.org/10.1126/science.1212858

70. N. Han, M. Race, W. Zhang, R. Marotta, C. Zhang et al., Perovskite and related oxide based electrodes for water splitting. J. Clean Prod. **318**, 128544 (2021). https://doi.org/10.1016/j.jclepro.2021.128544

71. C. Zhang, F. Wang, M. Batool, B. Xiong, H. Yang, Phase transition of $SrCo_{0.9}Fe_{0.1}O_3$ electrocatalysts and their effects on oxygen evolution reaction. SusMat **2**, 445–455 (2022). https://doi.org/10.1002/sus2.72

72. X. Xu, Y. Zhong, Z. Shao, Double perovskites in catalysis, electrocatalysis, and photo(electro)catalysis. Trends Chem. **1**(4), 410–424 (2019). https://doi.org/10.1016/j.trechm.2019.05.006

73. H. Sun, Z. Hu, X. Xu, J. He, J. Dai et al., Ternary phase diagram-facilitated rapid screening of double perovskites as electrocatalysts for the oxygen evolution reaction. Chem. Mater. **31**(15), 5919–5926 (2019). https://doi.org/10.1021/acs.chemmater.9b02261

74. C. Wei, Z. Feng, G.G. Scherer, J. Barber, Y. Shao-Horn et al., Cations in octahedral sites: a descriptor for oxygen electrocatalysis on transition-metal spinels. Adv. Mater. **29**(23), 1606800 (2017). https://doi.org/10.1002/adma.201606800

75. N. Han, S. Feng, W. Guo, O.M. Mora, X. Zhao et al., Rational design of ruddlesden–popper perovskite electrocatalyst for oxygen reduction to hydrogen peroxide. SusMat **2**(4), 456–465 (2022). https://doi.org/10.1002/sus2.71

76. Y. Zhu, H.A. Tahini, Z. Hu, Y. Yin, Q. Lin et al., Boosting oxygen evolution reaction by activation of Lattice-Oxygen sites in layered ruddlesden-popper oxide. EcoMat **2**(2), e12021 (2020). https://doi.org/10.1002/eom2.12021

77. J. Kim, P.-C. Shih, K.-C. Tsao, Y.-T. Pan, X. Yin et al., High-performance pyrochlore-type yttrium ruthenate electrocatalyst for oxygen evolution reaction in acidic media. J. Am. Chem. Soc. **139**(34), 12076–12083 (2017). https://doi.org/10.1021/jacs.7b06808

78. J. Song, C. Wei, Z.-F. Huang, C. Liu, L. Zeng et al., A review on fundamentals for designing oxygen evolution electrocatalysts. Chem. Soc. Rev. **49**(7), 2196–2214 (2020). https://doi.org/10.1039/C9CS00607A

79. N. Han, W. Zhang, W. Guo, S. Xie, C. Zhang et al., Novel oxygen permeable hollow fiber perovskite membrane with surface wrinkles. Sep. Purif. Technol. **261**, 118295–118316 (2021). https://doi.org/10.1016/j.seppur.2020.118295

80. Y. Liang, Y. Cui, Y. Chao, N. Han, J. Sunarso et al., Exsolution of cofe(Ru) nanoparticles in Ru-doped $(La_{0.8}Sr_{0.2})_{0.9}Co_{0.1}Fe_{0.8}Ru_{0.1}O_{3-\delta}$ for efficient oxygen evolution reaction. Nano Res. **15**, 6977–6986 (2022). https://doi.org/10.1007/s12274-022-4328-0

81. N. Han, C. Zhang, X. Tan, Z. Wang, S. Kawi et al., Re-evaluation of $La_{0.6}Sr_{0.4}Co_{0.2}Fe_{0.8}O_{3-\delta}$ hollow fiber membranes for oxygen separation after long-term storage of five and ten years. J. Mem. Sci. **587**, 117180 (2019). https://doi.org/10.1016/j.memsci.2019.117180

82. N. Han, S. Wang, Z. Yao, W. Zhang, X. Zhang et al., Superior three-dimensional perovskite catalyst for catalytic oxidation. EcoMat **2**(3), e12044 (2020). https://doi.org/10.1002/eom2.12044

83. L. Wang, K.A. Stoerzinger, L. Chang, J. Zhao, Y. Li et al., Tuning bifunctional oxygen electrocatalysts by changing the a-site rare-earth element in perovskite nickelates. Adv. Funct. Mater. **28**(39), 1803712 (2018). https://doi.org/10.1002/adfm.201803712

84. Y. Zhu, W. Zhou, J. Sunarso, Y. Zhong, Z. Shao, Phosphorus-doped perovskite oxide as highly efficient water oxidation electrocatalyst in alkaline solution. Adv. Funct. Mater. **26**(32), 5862–5872 (2016). https://doi.org/10.1002/adfm.201601902

85. X. Xu, Y. Chen, W. Zhou, Z. Zhu, C. Su et al., A perovskite electrocatalyst for efficient hydrogen evolution reaction. Adv. Mater. **28**(30), 6442–6448 (2016). https://doi.org/10.1002/adma.201600005

86. A. Sheelam, S. Balu, A. Muneeb, K.S. Bayikadi, D. Namasivayam et al., Improved oxygen redox activity by high-valent fe and Co^{3+} sites in the perovskite $LaNi_{1-x}Fe_{0.5x}Co_{0.5x}O3$. ACS Appl. Energ. Mater. **5**(1), 343–354 (2022). https://doi.org/10.1021/acsaem.1c02871

87. S. She, J. Yu, W. Tang, Y. Zhu, Y. Chen et al., Systematic study of oxygen evolution activity and stability on $La_{1-x}Sr_xFeO_{3-\delta}$ perovskite electrocatalysts in alkaline media. ACS Appl. Mater. Interfaces **10**(14), 11715–11721 (2018). https://doi.org/10.1021/acsami.8b00682

88. X. Cheng, E. Fabbri, Y. Yamashita, I.E. Castelli, B. Kim et al., Oxygen evolution reaction on perovskites: a multieffect descriptor study combining experimental and theoretical methods. ACS Catal. **8**(10), 9567–9578 (2018). https://doi.org/10.1021/acscatal.8b02022

89. X. Rong, J. Parolin, A.M. Kolpak, A fundamental relationship between reaction mechanism and stability in metal oxide catalysts for oxygen evolution. ACS Catal. **6**(2), 1153–1158 (2016). https://doi.org/10.1021/acscatal.5b02432

90. Y. Guo, Y. Tong, P. Chen, K. Xu, J. Zhao et al., Engineering the electronic state of a perovskite electrocatalyst for synergistically enhanced oxygen evolution reaction. Adv. Mater. **27**(39), 5989–5994 (2015). https://doi.org/10.1002/adma.201502024

91. Y. Zhu, H.A. Tahini, Z. Hu, Z.-G. Chen, W. Zhou et al., Boosting oxygen evolution reaction by creating both metal ion and lattice-oxygen active sites in a complex oxide. Adv. Mater. **32**(1), 1905025 (2020). https://doi.org/10.1002/adma.201905025

92. C. Bloed, J. Vuong, A. Enriquez, S. Raghavan, I. Tran et al., Oxygen vacancy and chemical ordering control oxygen evolution activity of $Sr_{2-x}Ca_xFe_2O_{6-\delta}$ perovskites. ACS Appl. Energ. Mater. **2**, 6140–6145 (2019). https://doi.org/10.1021/acsaem.9b00581

93. S. She, Y. Zhu, Y. Chen, Q. Lu, W. Zhou et al., Realizing ultrafast oxygen evolution by introducing proton acceptor into perovskites. Adv. Energ. Mater. **9**(20), 1900429 (2019). https://doi.org/10.1002/aenm.201900429

94. Y. Zhu, W. Zhou, Y. Zhong, Y. Bu, X. Chen et al., A perovskite nanorod as bifunctional electrocatalyst for overall water splitting. Adv. Energ. Mater. **7**(8), 1602122 (2017). https://doi.org/10.1002/aenm.201602122

95. Y. Zhu, W. Zhou, Z. Shao, Perovskite/carbon composites: applications in oxygen electrocatalysis. Small **13**(12), 1602122 (2017). https://doi.org/10.1002/aenm.201602122

96. P. Sabatier, Hydrogénations et déshydrogénations par catalyse. Ber. Dtsch. Chem. Ges. **44**(3), 1984–2001 (1911). https://doi.org/10.1002/cber.19110440303

97. J.S. Yoo, X. Rong, Y. Liu, A.M. Kolpak, Role of lattice oxygen participation in understanding trends in the oxygen evolution reaction on perovskites. ACS Catal. **8**(5), 4628–4636 (2018). https://doi.org/10.1021/acscatal.8b00612

98. A. Grimaud, O. Diaz-Morales, B. Han, W.T. Hong, Y.-L. Lee et al., Activating lattice oxygen redox reactions in metal oxides to catalyse oxygen evolution. Nat. Chem. **9**(5), 457–465 (2017). https://doi.org/10.1038/nchem.2695

99. E. Fabbri, M. Nachtegaal, T. Binninger, X. Cheng, B.-J. Kim et al., Dynamic surface self-reconstruction is the key of highly active perovskite nano-electrocatalysts for water splitting. Nat. Mater. **16**(9), 925–931 (2017). https://doi.org/10.1038/nmat4938

100. Y. Zhu, H.A. Tahini, Z. Hu, Y. Yin, Q. Lin et al., Boosting oxygen evolution reaction by activation of lattice-oxygen sites in layered ruddlesden-popper oxide. EcoMat (2020). https://doi.org/10.1002/eom2.12021

101. D.A. Kuznetsov, M.A. Naeem, P.V. Kumar, P.M. Abdala, A. Fedorov et al., Tailoring lattice oxygen binding in ruthenium pyrochlores to enhance oxygen evolution activity. J. Am. Chem. Soc. **142**(17), 7883–7888 (2020). https://doi.org/10.1021/jacs.0c01135

102. Y. Yao, S. Hu, W. Chen, Z.-Q. Huang, W. Wei et al., Engineering the electronic structure of single atom ru sites via compressive strain boosts acidic water oxidation electrocatalysis. Nat. Catal. **2**(4), 304–313 (2019). https://doi.org/10.1038/s41929-019-0246-2

103. M. Shao, Q. Chang, J.-P. Dodelet, R. Chenitz, Recent advances in electrocatalysts for oxygen reduction reaction. Chem. Rev. **116**(6), 3594–3657 (2016). https://doi.org/10.1021/acs.chemrev.5b00462

104. J. Suntivich, H.A. Gasteiger, N. Yabuuchi, H. Nakanishi, J.B. Goodenough et al., Design principles for oxygen-reduction activity on perovskite oxide catalysts for fuel cells and metal–air batteries. Nat. Chem. **3**(7), 546–550 (2011)

105. J. Lim, D. Park, S.S. Jeon, C.-W. Roh, J. Choi et al., Ultrathin IrO_2 nanoneedles for electrochemical water oxidation. Adv. Funct. Mater. **28**(4), 1704796 (2018). https://doi.org/10.1002/adfm.201704796

106. S. Laha, Y. Lee, F. Podjaski, D. Weber, V. Duppel et al., Ruthenium oxide nanosheets for enhanced oxygen evolution catalysis in acidic medium. Adv. Energ. Mater. **9**(15), 1803795 (2019). https://doi.org/10.1002/aenm.201803795

107. A. Bergmann, E. Martinez-Moreno, D. Teschner, P. Chernev, M. Gliech et al., Reversible amorphization and the catalytically active state of crystalline Co_3O_4 during oxygen evolution. Nat. Commun. **6**(1), 8625 (2015). https://doi.org/10.1038/ncomms9625

108. Y. Chen, H. Li, J. Wang, Y. Du, S. Xi et al., Exceptionally active iridium evolved from a pseudo-cubic perovskite for oxygen evolution in acid. Nat. Commun. **10**(1), 572 (2019)

109. D. Chen, M. Qiao, Y.-R. Lu, L. Hao, D. Liu et al., Preferential cation vacancies in perovskite hydroxide for the oxygen evolution reaction. Angew. Chem. Int. Ed. **57**(28), 8691–8696 (2018). https://doi.org/10.1002/anie.201805520

110. J.R. Petrie, V.R. Cooper, J.W. Freeland, T.L. Meyer, Z. Zhang et al., Enhanced bifunctional oxygen catalysis in strained $LaNiO_3$ perovskites. J. Am. Chem. Soc. **138**(8), 2488–2491 (2016). https://doi.org/10.1021/jacs.5b11713

111. K.A. Stoerzinger, W.S. Choi, H. Jeen, H.N. Lee, Y. Shao-Horn, Role of strain and conductivity in oxygen electrocatalysis on $LaCoO_3$ thin films. J. Phy. Chem. Lett. **6**(3), 487–492 (2015). https://doi.org/10.1021/jz502692a

112. J. Chen, H. Hu, F. Meng, T. Yajima, L. Yang et al., Overlooked transportation anisotropies in d-band correlated rare-earth perovskite nickelates. Matter **2**(5), 1296–1306 (2020). https://doi.org/10.1016/j.matt.2020.02.023

113. D.A. Kuznetsov, B. Han, Y. Yu, R.R. Rao, J. Hwang et al., Tuning redox transitions via inductive effect in metal oxides and complexes, and implications in oxygen electrocatalysis. Joule **2**(2), 225–244 (2018). https://doi.org/10.1016/j.joule.2017.11.014

114. C. Guo, Y. Zheng, J. Ran, F. Xie, M. Jaroniec et al., Engineering high-energy interfacial structures for high-performance oxygen-involving electrocatalysis. Angew. Chem. Int. Ed. **56**(29), 8539–8543 (2017). https://doi.org/10.1002/anie.201701531

115. L.C. Seitz, C.F. Dickens, K. Nishio, Y. Hikita, J. Montoya et al., A highly active and stable IrO_x/$SrIrO_3$ catalyst for the oxygen evolution reaction. Science **353**(6303), 1011–1014 (2016). https://doi.org/10.1126/science.aaf5050%JScience

116. Z. Li, J. Yang, Z. Chen, C. Zheng, L.Q. Wei et al., V "bridged" Co to eliminate charge transfer barriers and drive lattice oxygen oxidation during water-splitting. Adv. Funct. Mater. **31**(9), 2008822 (2021). https://doi.org/10.1002/adfm.202008822

117. Y. Liu, Y. Ying, L. Fei, Y. Liu, Q. Hu et al., Valence engineering via selective atomic substitution on tetrahedral sites in spinel oxide for highly enhanced oxygen evolution catalysis. J. Am. Chem. Soc. **141**(20), 8136–8145 (2019). https://doi.org/10.1021/jacs.8b13701

118. M. Xu, H. Sun, W. Wang, Y. Shen, W. Zhou et al., Scandium and phosphorus co-doped perovskite oxides as high-performance electrocatalysts for the oxygen reduction reaction in an alkaline solution. J. Mater. Sci. Technol. **39**, 22–27 (2020). https://doi.org/10.1016/j.jmst.2019.09.007

119. A. Zunger, O.I. Malyi, Understanding doping of quantum materials. Chem. Rev. **121**(5), 3031–3060 (2021). https://doi.org/10.1021/acs.chemrev.0c00608

120. Y. Lin, Z. Tian, L. Zhang, J. Ma, Z. Jiang et al., Chromium-ruthenium oxide solid solution electrocatalyst for highly efficient oxygen evolution reaction in acidic media.

Nat. Commun. **10**(1), 162 (2019). https://doi.org/10.1038/s41467-018-08144-3

121. J. Su, R. Ge, K. Jiang, Y. Dong, F. Hao et al., Assembling ultrasmall copper-doped ruthenium oxide nanocrystals into hollow porous polyhedra: highly robust electrocatalysts for oxygen evolution in acidic media. Adv. Mater. **30**(29), 1801351 (2018). https://doi.org/10.1002/adma.201801351

122. S. Chen, H. Huang, P. Jiang, K. Yang, J. Diao et al., Mn-doped RuO_2 nanocrystals as highly active electrocatalysts for enhanced oxygen evolution in acidic media. ACS Catal. **10**(2), 1152–1160 (2020). https://doi.org/10.1021/acscatal.9b04922

123. Y. Wang, S. Hao, X. Liu, Q. Wang, Z. Su et al., Ce-doped IrO_2 electrocatalysts with enhanced performance for water oxidation in acidic media. ACS Appl. Mater. Interfaces **12**(33), 37006–37012 (2020). https://doi.org/10.1021/acsami.0c00389

124. Z. Li, S. Wang, Y. Tian, B. Li, H.J. Yan et al., Mg-doping improves the performance of Ru-based electrocatalysts for the acidic oxygen evolution reaction. Chem. Commun. **56**(11), 1749–1752 (2020). https://doi.org/10.1039/C9CC09613B

125. X. Cheng, E. Fabbri, M. Nachtegaal, I.E. Castelli, M. El Kazzi et al., Oxygen evolution reaction on $La_{1-x}Sr_xCoO_3$ perovskites: a combined experimental and theoretical study of their structural, electronic, and electrochemical properties. Chem. Mater. **27**(22), 7662–7672 (2015). https://doi.org/10.1021/acs.chemmater.5b03138

126. J.-I. Jung, H.Y. Jeong, J.-S. Lee, M.G. Kim, J. Cho, A bifunctional perovskite catalyst for oxygen reduction and evolution. Angew. Chem. Int. Ed. **53**(18), 4582–4586 (2014). https://doi.org/10.1002/anie.201311223

127. Z. Wu, L.-P. Sun, T. Xia, L.-H. Huo, H. Zhao et al., Effect of sr doping on the electrochemical properties of bi-functional oxygen electrode $PrBa_{1-x}Sr_xCo_2O_{5+\delta}$. J. Power Sources **334**, 86–93 (2016). https://doi.org/10.1016/j.jpowsour.2016.10.013

128. N. Han, S. Feng, Y. Liang, J. Wang, W. Zhang et al., Achieving efficient electrocatalytic oxygen evolution in acidic media on yttrium ruthenate pyrochlore through cobalt incorporation. Adv. Funct. Mater. (2023). https://doi.org/10.1002/adfm.202208399

129. S. She, Y. Zhu, X. Wu, Z. Hu, A. Shelke et al., Realizing high and stable electrocatalytic oxygen evolution for iron-based perovskites by co-doping-induced structural and electronic modulation. Adv. Funct. Mater. **32**(15), 2111091 (2022). https://doi.org/10.1002/adfm.202111091

130. Q. Lu, X. Zou, X. Wang, L. An, Z. Shao et al., Simultaneous reactant accessibility and charge transfer engineering in Co-doped RuO_2-supported ocnt for robust rechargeable zinc-air batteries. Appl. Catal. B-Environ. **325**, 122323 (2023). https://doi.org/10.1016/j.apcatb.2022.122323

131. T.D. Nguyen, H.H. Nguyen, C. Dai, J. Wang, G.G. Scherer, Activity and stability optimization of $Ru_xIr_{1-x}O_2$ nanocatalyst for the oxygen evolution reaction by tuning the synthetic process. Int. J. Hydrogen. Energ. **45**(1), 46–55 (2020). https://doi.org/10.1016/j.ijhydene.2019.10.179

132. J. Feng, F. Lv, W. Zhang, P. Li, K. Wang et al., Iridium-based multimetallic porous hollow nanocrystals for efficient overall-water-splitting catalysis. Adv. Mater. **29**(47), 1703798 (2017). https://doi.org/10.1002/adma.201703798

133. W. Sun, Y. Song, X.-Q. Gong, L.-M. Cao, J. Yang, An efficiently tuned d-orbital occupation of IrO_2 by doping with cu for enhancing the oxygen evolution reaction activity. Chem. Sci. **6**(8), 4993–4999 (2015). https://doi.org/10.1039/C5SC01251A

134. F. Lv, J. Feng, K. Wang, Z. Dou, W. Zhang et al., Iridium–tungsten alloy nanodendrites as pH-universal water-splitting electrocatalysts. ACS Cent. Sci. **4**(9), 1244–1252 (2018). https://doi.org/10.1021/acscentsci.8b00426

135. R. Ge, L. Li, J. Su, Y. Lin, Z. Tian et al., Ultrafine defective RuO_2 electrocatayst integrated on carbon cloth for robust water oxidation in acidic media. Adv. Energ. Mater. **9**(35), 1901313 (2019). https://doi.org/10.1002/aenm.201901313

136. J. Suntivich, W.T. Hong, Y.-L. Lee, J.M. Rondinelli, W. Yang et al., Estimating hybridization of transition metal and oxygen states in perovskites from o K-edge X-ray absorption spectroscopy. J. Phy. Chem. C **118**(4), 1856–1863 (2014). https://doi.org/10.1021/jp410644j

137. W.-J. Yin, B. Weng, J. Ge, Q. Sun, Z. Li et al., Oxide perovskites, double perovskites and derivatives for electrocatalysis, photocatalysis, and photovoltaics. Energy Environ. Sci. **12**(2), 442–462 (2019). https://doi.org/10.1039/C8EE01574K

138. M. Retuerto, L. Pascual, F. Calle-Vallejo, P. Ferrer, D. Gianolio et al., Na-doped ruthenium perovskite electrocatalysts with improved oxygen evolution activity and durability in acidic media. Nat. Commun. **10**(1), 2041 (2019). https://doi.org/10.1038/s41467-019-09791-w

139. B.S. Yeo, A.T. Bell, Enhanced activity of gold-supported cobalt oxide for the electrochemical evolution of oxygen. J. Am. Chem. Soc. **133**(14), 5587–5593 (2011). https://doi.org/10.1021/ja200559j

140. X. Xu, Y. Pan, L. Ge, Y. Chen, X. Mao et al., High-performance perovskite composite electrocatalysts enabled by controllable interface engineering. Small **17**(29), 2101573 (2021). https://doi.org/10.1002/smll.202101573

141. X. Xu, W. Wang, W. Zhou, Z. Shao, Recent advances in novel nanostructuring methods of perovskite electrocatalysts for energy-related applications. Small Methods **2**(7), 1800071 (2018). https://doi.org/10.1002/smtd.201800071

142. J. Suntivich, K.J. May, H.A. Gasteiger, J.B. Goodenough, Y. Shao-Horn, A perovskite oxide optimized for oxygen evolution catalysis from molecular orbital principles. Science **334**(6061), 1383–1385 (2011). https://doi.org/10.1126/science.1212858

143. J. Rossmeisl, Z.W. Qu, H. Zhu, G.J. Kroes, J.K. Nørskov, Electrolysis of water on oxide surfaces. J. Electroanal. Chem. **607**(1), 83–89 (2007). https://doi.org/10.1016/j.jelechem.2006.11.008

144. J.B. Goodenough, R. Manoharan, M. Paranthaman, Surface protonation and electrochemical activity of oxides in aqueous solution. J. Am. Chem. Soc. **112**(6), 2076–2082 (1990). https://doi.org/10.1021/ja00162a006

145. J. Kim, X. Yin, K.-C. Tsao, S. Fang, H. Yang, $Ca_2Mn_2O_5$ as oxygen-deficient perovskite electrocatalyst for oxygen evolution reaction. J. Am. Chem. Soc. **136**(42), 14646–14649 (2014). https://doi.org/10.1021/ja506254g

146. J.G. Lee, J. Hwang, H.J. Hwang, O.S. Jeon, J. Jang et al., A new family of perovskite catalysts for oxygen-evolution reaction in alkaline media: BaNiO3 and $BaNi_{0.83}O_{2.5}$. J. Am. Chem. Soc. **138**(10), 3541–3547 (2016). https://doi.org/10.1021/jacs.6b00036

147. Y. Zhou, S. Sun, S. Xi, Y. Duan, T. Sritharan et al., Superexchange effects on oxygen reduction activity of edge-sharing $[Co_xMn_{1-x}O_6]$ octahedra in spinel oxide. Adv. Mater. **30**(11), 1705407 (2018). https://doi.org/10.1002/adma.201705407

148. Y. Zhu, W. Zhou, J. Yu, Y. Chen, M. Liu et al., Enhancing electrocatalytic activity of perovskite oxides by tuning cation deficiency for oxygen reduction and evolution reactions. Chem. Mater. **28**(6), 1691–1697 (2016). https://doi.org/10.1021/acs.chemmater.5b04457

149. J. Huang, J. Chen, T. Yao, J. He, S. Jiang et al., CoOOH nanosheets with high mass activity for water oxidation. Angew. Chem. Int. Ed. **54**(30), 8722–8727 (2015). https://doi.org/10.1002/anie.201502836

150. C. Su, W. Wang, Y. Chen, G. Yang, X. Xu et al., $SrCo_{0.9}Ti_{0.1}O_{3-\delta}$ as a new electrocatalyst for the oxygen evolution reaction in alkaline electrolyte with stable performance. ACS Appl. Mater. Interfaces **7**(32), 17663–17670 (2015). https://doi.org/10.1021/acsami.5b02810

151. Y.-Q. Lyu, F. Ciucci, Activating the bifunctionality of a perovskite oxide toward oxygen reduction and oxygen evolution reactions. ACS Appl. Mater. Interfaces **9**(41), 35829–35836 (2017). https://doi.org/10.1021/acsami.7b10216

152. B. Zhao, L. Zhang, D. Zhen, S. Yoo, Y. Ding et al., A tailored double perovskite nanofiber catalyst enables ultrafast oxygen evolution. Nat. Commun. **8**(1), 14586 (2017). https://doi.org/10.1038/ncomms14586

153. C.E. Beall, E. Fabbri, T.J. Schmidt, Perovskite oxide based electrodes for the oxygen reduction and evolution reactions: the underlying mechanism. ACS Catal. **11**(5), 3094–3114 (2021). https://doi.org/10.1021/acscatal.0c04473

154. J.M. Rondinelli, S.J. May, Deliberate deficiencies: expanding electronic function through non-stoichiometry. Matter **1**(1), 33–35 (2019). https://doi.org/10.1016/j.matt.2019.06.013

155. Z. Chen, N. Han, R. Zheng, Z. Ren, W. Wei et al., Design of earth-abundant amorphous transition metal-based catalysts for electrooxidation of small molecules: advances and perspectives. SusMat (2023). https://doi.org/10.1002/sus2.131

156. G. Jia, Y. Wang, X. Cui, H. Zhang, J. Zhao et al., Wet-chemistry hydrogen doped TiO_2 with switchable defects control for photocatalytic hydrogen evolution. Matter **5**(1), 206–218 (2022). https://doi.org/10.1016/j.matt.2021.10.027

157. S.C. Perry, D. Pangotra, L. Vieira, L.-I. Csepei, V. Sieber et al., Electrochemical synthesis of hydrogen peroxide from water and oxygen. Nat. Rev. Chem. **3**(7), 442–458 (2019)

158. K.A. Stoerzinger, M. Risch, B. Han, Y. Shao-Horn, Recent insights into manganese oxides in catalyzing oxygen reduction kinetics. ACS Catal. **5**(10), 6021–6031 (2015). https://doi.org/10.1021/acscatal.5b01444

159. A. Kulkarni, S. Siahrostami, A. Patel, J.K. Nørskov, Understanding catalytic activity trends in the oxygen reduction reaction. Chem. Rev. **118**(5), 2302–2312 (2018). https://doi.org/10.1021/acs.chemrev.7b00488

160. Y. Xu, X. Liu, N. Cao, X. Xu, L. Bi, Defect engineering for electrocatalytic nitrogen reduction reaction at ambient conditions. Sustain. Mater. Technol. **27**, e00229 (2021). https://doi.org/10.1016/j.susmat.2020.e00229

161. J. Chen, W. Zhang, H. Li, W. Li, D. Zhao, Recent advances in TiO_2-based catalysts for N_2 reduction reaction. SusMat **1**(2), 174–193 (2021). https://doi.org/10.1002/sus2.13

162. W. Shi, H. Liu, Z. Li, C. Li, J. Zhou et al., High-entropy alloy stabilized and activated pt clusters for highly efficient electrocatalysis. SusMat **2**(2), 186–196 (2022). https://doi.org/10.1002/sus2.56

163. Y. Tian, S. Wang, E. Velasco, Y. Yang, L. Cao et al., A Co-doped nanorod-like RuO_2 electrocatalyst with abundant oxygen vacancies for acidic water oxidation. Science **23**(1), 100756–100816 (2020). https://doi.org/10.1016/j.isci.2019.100756

164. Q. Ji, L. Bi, J. Zhang, H. Cao, X.S. Zhao, The role of oxygen vacancies of ABO_3 perovskite oxides in the oxygen reduction reaction. Energ. Environ. Sci. **13**(5), 1408–1428 (2020). https://doi.org/10.1039/D0EE00092B

165. M.A. Peña, J.L.G. Fierro, Chemical structures and performance of perovskite oxides. Chem. Rev. **101**(7), 1981–2018 (2001). https://doi.org/10.1021/cr980129f

166. K. Conder, E. Pomjakushina, A. Soldatov, E. Mitberg, Oxygen content determination in perovskite-type cobaltates. Mater. Res. Bull. **40**(2), 257–263 (2005). https://doi.org/10.1016/j.materresbull.2004.10.009

167. J.T. Mefford, X. Rong, A.M. Abakumov, W.G. Hardin, S. Dai et al., Water electrolysis on $La_{1-x}Sr_xCoO_{3-\delta}$ perovskite electrocatalysts. Nat. Commun. **7**(1), 11053 (2016). https://doi.org/10.1038/ncomms11053

168. Y. Jiang, Z. Geng, L. Yuan, Y. Sun, Y. Cong et al., Nanoscale architecture of $Ru_{O.2}/La_{0.9}Fe_{0.92}Ru_{0.08}-xO_{3-\delta}$ composite via manipulating the exsolution of low Ru-substituted a-site deficient perovskite. ACS Sustain. Chem. Eng. **6**(9), 11999–12005 (2018). https://doi.org/10.1021/acssuschemeng.8b02288

169. Y. Zhu, J. Dai, W. Zhou, Y. Zhong, H. Wang et al., Synergistically enhanced hydrogen evolution electrocatalysis by in-situ exsolution of metallic nanoparticles on perovskites. J. Mater. Chem. A **6**, 13582–13587 (2018). https://doi.org/10.1039/C8TA02347F

170. X. Xu, Y. Chen, W. Zhou, Y. Zhong, D. Guan et al., Earth-abundant silicon for facilitating water oxidation over

Iron-based perovskite electrocatalyst. Adv. Mater. Interfaces **5**, 1701693 (2018). https://doi.org/10.1002/admi.201701693

171. T. Ling, D.-Y. Yan, H. Wang, Y. Jiao, Z. Hu et al., Activating cobalt(ii) oxide nanorods for efficient electrocatalysis by strain engineering. Nat. Commun. **8**(1), 1509 (2017). https://doi.org/10.1038/s41467-017-01872-y

172. J. Hwang, Z. Feng, N. Charles, X.R. Wang, D. Lee et al., Tuning perovskite oxides by strain: electronic structure, properties, and functions in (electro)catalysis and ferroelectricity. Mater. Today **31**, 100–118 (2019). https://doi.org/10.1016/j.mattod.2019.03.014

173. D. Pesquera, G. Herranz, A. Barla, E. Pellegrin, F. Bondino et al., Surface symmetry-breaking and strain effects on orbital occupancy in transition metal perovskite epitaxial films. Nat. Commun. **3**(1), 1189 (2012). https://doi.org/10.1038/ncomms2189

174. J.M. Rondinelli, N.A. Spaldin, Structure and properties of functional oxide thin films: insights from electronic-structure calculations. Adv. Mater. **23**(30), 3363–3381 (2011). https://doi.org/10.1002/adma.201101152

175. S.A. Akhade, J.R. Kitchin, Effects of strain, d-band filling, and oxidation state on the surface electronic structure and reactivity of 3d perovskite surfaces. J. Chem. Phy. **137**(8), 084703 (2012). https://doi.org/10.1063/1.4746117

176. D. Lee, R. Jacobs, Y. Jee, A. Seo, C. Sohn et al., Stretching epitaxial $La_{0.6}Sr_{0.4}CoO_{3-\delta}$ for fast oxygen reduction. J. Phy. Chem. C **121**(46), 25651–25658 (2017). https://doi.org/10.1021/acs.jpcc.7b06374

177. R. Jacobs, J. Booske, D. Morgan, Understanding and controlling the work function of perovskite oxides using density functional theory. Adv. Funct. Mater. **26**(30), 5471–5482 (2016). https://doi.org/10.1002/adfm.201600243

178. X. Li, H. Liu, Z. Chen, Q. Wu, Z. Yu, Enhancing oxygen evolution efficiency of multiferroic oxides by spintronic and ferroelectric polarization regulation. Nat. Commun. **10**(1), 1409 (2019). https://doi.org/10.1038/s41467-019-09191-0

179. K.J. Choi, M. Biegalski, Y.L. Li, A. Sharan, J. Schubert et al., Enhancement of ferroelectricity in strained $BaTiO_3$ thin films. Science **306**(5698), 1005–1009 (2004). https://doi.org/10.1126/science.1103218

180. T. Mayeshiba, D. Morgan, Strain effects on oxygen migration in perovskites. Phys. Chem. Chem. Phys. **17**(4), 2715–2721 (2015). https://doi.org/10.1039/C4CP05554C

181. M. Kubicek, Z. Cai, W. Ma, B. Yildiz, H. Hutter et al., Tensile lattice strain accelerates oxygen surface exchange and diffusion in $La_{1-x}Sr_xCoO_{3-\delta}$ thin films. ACS Nano **7**(4), 3276–3286 (2013). https://doi.org/10.1021/nn305987x

182. S. Stemmer, A.J. Jacobson, X. Chen, A. Ignatiev, Oxygen vacancy ordering in epitaxial $La_{0.5}Sr_{0.5}CoO_{3-\delta}$ thin films on (001) LaAlO3. J. Appl. Phys. **90**(7), 3319–3324 (2001). https://doi.org/10.1063/1.1401793

183. T.T. Mayeshiba, D.D. Morgan, Factors controlling oxygen migration barriers in perovskites. Solid State Ionics **296**, 71–77 (2016). https://doi.org/10.1016/j.ssi.2016.09.007

184. S. Xu, R. Jacobs, D. Morgan, Factors controlling oxygen interstitial diffusion in the Ruddlesden–popper oxide $La_{2-x}Sr_xNiO_{4+\delta}$. Chem. Mater. **30**(20), 7166–7177 (2018). https://doi.org/10.1021/acs.chemmater.8b03146

185. T.L. Meyer, R. Jacobs, D. Lee, L. Jiang, J.W. Freeland et al., Strain control of oxygen kinetics in the Ruddlesden-popper oxide $La_{1.85}Sr_{0.15}CuO_4$. Nat. Commun. **9**(1), 92 (2018). https://doi.org/10.1038/s41467-017-02568-z

186. N. Han, X. Guo, J. Cheng, P. Liu, S. Zhang et al., Inhibiting in situ phase transition in ruddlesden-popper perovskite via tailoring bond hybridization and its application in oxygen permeation. Matter **4**(5), 1720–1734 (2021). https://doi.org/10.1016/j.matt.2021.02.019

187. R. Jacobs, J. Hwang, Y. Shao-Horn, D. Morgan, Assessing correlations of perovskite catalytic performance with electronic structure descriptors. Chem. Mater. **31**(3), 785–797 (2019). https://doi.org/10.1021/acs.chemmater.8b03840

188. Y.-L. Lee, M.J. Gadre, Y. Shao-Horn, D. Morgan, Ab initio gga+u study of oxygen evolution and oxygen reduction electrocatalysis on the (001) surfaces of lanthanum transition metal perovskites $LaBO_3$ (b=Cr, Mn, Fe, Co and Ni). Phys. Chem. Chem. Phys. **17**(33), 21643–21663 (2015). https://doi.org/10.1039/C5CP02834E

189. M. Risch, K.A. Stoerzinger, S. Maruyama, W.T. Hong, I. Takeuchi et al., $La_{0.8}Sr_{0.2}MnO_{3-\delta}$ decorated with $Ba_{0.5}Sr_{0.5}Co_{0.8}Fe_{0.2}O_{3-\delta}$: a bifunctional surface for oxygen electrocatalysis with enhanced stability and activity. J. Am. Chem. Soc. **136**(14), 5229–5232 (2014). https://doi.org/10.1021/ja5009954

190. J.R. Petrie, C. Mitra, H. Jeen, W.S. Choi, T.L. Meyer et al., Strain control of oxygen vacancies in epitaxial strontium cobaltite films. Adv. Funct. Mater. **26**(10), 1564–1570 (2016). https://doi.org/10.1002/adfm.201504868

191. J.R. Petrie, H. Jeen, S.C. Barron, T.L. Meyer, H.N. Lee, Enhancing perovskite electrocatalysis through strain tuning of the oxygen deficiency. J. Am. Chem. Soc. **138**(23), 7252–7255 (2016). https://doi.org/10.1021/jacs.6b03520

192. Z. Chen, S. Yun, L. Wu, J. Zhang, X. Shi et al., Waste-derived catalysts for water electrolysis: circular economy-driven sustainable green hydrogen energy. Nano-Micro Lett. **15**(1), 4 (2022). https://doi.org/10.1007/s40820-022-00974-7

193. J. Li, Oxygen evolution reaction in energy conversion and storage: design strategies under and beyond the energy scaling relationship. Nano-Micro Lett. **14**(1), 112 (2022). https://doi.org/10.1007/s40820-022-00857-x

194. X. Xu, Z. Shao, S.P. Jiang, High-entropy materials for water electrolysis. Energy Technol. **10**(11), 2200573 (2022). https://doi.org/10.1002/ente.202200573

195. P. Tan, R. Gao, Y. Zhang, N. Han, Y. Jiang et al., Electrostatically directed assembly of two-dimensional ultrathin $Co_2Ni-MoF/Ti_3C_2T_x$ nanosheets for electrocatalytic oxygen evolution. J. Colloid. Interf. Sci. **630**, 363–371 (2023). https://doi.org/10.1016/j.jcis.2022.10.109

196. H. Sun, S. Song, X. Xu, J. Dai, J. Yu et al., Recent progress on structurally ordered materials for electrocatalysis. Adv.

Energ. Mater. **11**(37), 2101937 (2021). https://doi.org/10.1002/aenm.202101937

197. Z. Liu, Z. Tang, Y. Song, G. Yang, W. Qian et al., High-entropy perovskite oxide: a new opportunity for developing highly active and durable air electrode for reversible protonic ceramic electrochemical cells. Nano-Micro Lett. **14**(1), 217 (2022). https://doi.org/10.1007/s40820-022-00967-6

198. Y. Dai, J. Yu, J. Wang, Z. Shao, D. Guan et al., Bridging the charge accumulation and high reaction order for high-rate oxygen evolution and long stable zn-air batteries. Adv. Funct. Mater. **32**(24), 2111989 (2022). https://doi.org/10.1002/adfm.202111989

199. H. Sun, X. Xu, H. Kim, W. Jung, W. Zhou et al., Electrochemical water splitting: bridging the gaps between fundamental research and industrial applications. Energ. Environ. Mater. (2023). https://doi.org/10.1002/eem2.12441

200. A.I. Douka, H. Yang, L. Huang, S. Zaman, T. Yue et al., Transition metal/carbon hybrids for oxygen electrocatalysis in rechargeable zinc-air batteries. EcoMat **3**(1), e12067 (2021). https://doi.org/10.1002/eom2.12067

201. C. Jin, X. Cao, L. Zhang, C. Zhang, R. Yang, Preparation and electrochemical properties of urchin-like $La_{0.8}Sr_{0.2}MnO_3$ perovskite oxide as a bifunctional catalyst for oxygen reduction and oxygen evolution reaction. J. Power Sources **241**, 225–230 (2013). https://doi.org/10.1016/j.jpowsour.2013.04.116

202. J. Bian, R. Su, Y. Yao, J. Wang, J. Zhou et al., Mg doped perovskite $LaNiO_3$ nanofibers as an efficient bifunctional catalyst for rechargeable zinc–air batteries. ACS Appl. Energ. Mater. **2**(1), 923–931 (2019). https://doi.org/10.1021/acsaem.8b02183

203. S. Bie, Y. Zhu, J. Su, C. Jin, S. Liu et al., One-pot fabrication of yolk–shell structured $La_{0.9}Sr_{0.1}CoO_3$ perovskite microspheres with enhanced catalytic activities for oxygen reduction and evolution reactions. J. Mater. Chem. A **3**(44), 22448–22453 (2015). https://doi.org/10.1039/C5TA05271H

204. C. Jin, Z. Yang, X. Cao, F. Lu, R. Yang, A novel bifunctional catalyst of $Ba_{0.9}Co_{0.5}Fe_{0.4}Nb_{0.1}O_{3-\delta}$ perovskite for lithium–air battery. Int. J. Hydrogen Energy **39**(6), 2526–2530 (2014). https://doi.org/10.1016/j.ijhydene.2013.12.003

205. Y. Xu, A. Tsou, Y. Fu, J. Wang, J.-H. Tian et al., Carbon-coated perovskite $BaMnO_3$ porous nanorods with enhanced electrocatalytic perporites for oxygen reduction and oxygen evolution. Electrochim. Acta **174**, 551–556 (2015). https://doi.org/10.1016/j.electacta.2015.05.184

206. X. Ge, B. Li, D. Wuu, A. Sumboja, T. An et al., Nanostructured perovskite $LaCo_{1-x}Mn_xO_3$ as bifunctional catalysts for rechargeable metal–air batteries. J. Mol. Eng. Mater. **3**, 1540006 (2015). https://doi.org/10.1142/s2251237315400067

207. C. Jin, X. Cao, F. Lu, Z. Yang, R. Yang, Electrochemical study of $Ba_{0.5}Sr_{0.5}Co_{0.8}Fe_{0.2}O_3$ perovskite as bifunctional catalyst in alkaline media. Int. J. Hydrogen Energy **38**(25), 10389–10393 (2013). https://doi.org/10.1016/j.ijhydene.2013.06.047

208. C.-F. Chen, G. King, R.M. Dickerson, P.A. Papin, S. Gupta et al., Oxygen-deficient $BaTiO_{3-x}$ perovskite as an efficient bifunctional oxygen electrocatalyst. Nano Energy **13**, 423–432 (2015). https://doi.org/10.1016/j.nanoen.2015.03.005

209. L. Yan, Y. Lin, X. Yu, W. Xu, T. Salas et al., $La_{0.8}Sr_{0.2}MnO_3$-based perovskite nanoparticles with the a-site deficiency as high performance bifunctional oxygen catalyst in alkaline solution. ACS Appl. Mater. Interfaces **9**(28), 23820–23827 (2017). https://doi.org/10.1021/acsami.7b06458

210. W. Xu, L. Yan, L. Teich, S. Liaw, M. Zhou et al., Polymer-assisted chemical solution synthesis of $La_{0.8}Sr_{0.2}MnO_3$-based perovskite with a-site deficiency and cobalt-doping for bifunctional oxygen catalyst in alkaline media. Electrochim. Acta **273**, 80–87 (2018). https://doi.org/10.1016/j.electacta.2018.04.046

211. H. Wang, W. Xu, S. Richins, K. Liaw, L. Yan et al., Polymer-assisted approach to $LaCo_{1-x}Ni_xO_3$ network nanostructures as bifunctional oxygen electrocatalysts. Electrochim. Acta **296**, 945–953 (2019). https://doi.org/10.1016/j.electacta.2018.11.075

212. M.Y. Oh, J.S. Jeon, J.J. Lee, P. Kim, K.S. Nahm, The bifunctional electrocatalytic activity of perovskite $La_{0.6}Sr_{0.4}CoO_{3-\delta}$ for oxygen reduction and evolution reactions. RSC Adv. **5**(25), 19190–19198 (2015). https://doi.org/10.1039/C4RA16097E

213. Y. Zhao, L. Xu, L. Mai, C. Han, Q. An et al., Hierarchical mesoporous perovskite $La_{0.5}Sr_{0.5}CoO_{2.91}$ nanowires with ultrahigh capacity for Li-air batteries. Proc. Natl. Acad. Sci. **109**(48), 19569–19574 (2012). https://doi.org/10.1073/pnas.1210315109

214. Z. Shao, S.M. Haile, A high-performance cathode for the next generation of solid-oxide fuel cells. Nature **431**(7005), 170–173 (2004)

215. Z. Shao, S.M. Haile, J. Ahn, P.D. Ronney, Z. Zhan et al., A thermally self-sustained micro solid-oxide fuel-cell stack with high power density. Nature **435**(7043), 795 (2005)

216. N. Han, W. Wang, S. Zhang, J. Sunarso, Z. Zhu et al., A novel heterogeneous $La_{0.8}Sr_{0.2}CoO_{3-\delta}/(La_{0.5}Sr_{0.5})2CoO_{4+\delta}$ dual-phase membrane for oxygen separation. Asia-Pac. J. Chem. Eng. **13**(5), e2239 (2018). https://doi.org/10.1002/apj.2239

217. N. Han, R. Chen, T. Chang, L. Li, H. Wang et al., A novel lanthanum strontium cobalt iron composite membrane synthesised through beneficial phase reaction for oxygen separation. Ceram. Int. **45**(15), 18924–18930 (2019). https://doi.org/10.1016/j.ceramint.2019.06.128

218. S. Dwivedi, Solid oxide fuel cell: materials for anode, cathode and electrolyte. Int. J. Hydrogen Energy **45**(44), 23988–24013 (2020). https://doi.org/10.1016/j.ijhydene.2019.11.234

219. Y. Zhang, X. Gao, J. Sunarso, B. Liu, W. Zhou et al., Significantly improving the durability of single-chamber solid oxide fuel cells: a highly active CO_2-resistant perovskite cathode. ACS Appl. Energ. Mater. **1**(3), 1337–1343 (2018). https://doi.org/10.1021/acsaem.8b00051

220. D. Chen, C. Chen, Z.M. Baiyee, Z. Shao, F. Ciucci, Non-stoichiometric oxides as low-cost and highly-efficient oxygen reduction/evolution catalysts for low-temperature electrochemical devices. Chem. Rev. **115**(18), 9869–9921 (2015). https://doi.org/10.1021/acs.chemrev.5b00073

221. Y. Song, W. Wang, L. Ge, X. Xu, Z. Zhang et al., Rational design of a water-storable hierarchical architecture decorated with amorphous barium oxide and nickel nanoparticles as a solid oxide fuel cell anode with excellent sulfur tolerance. Adv. Sci. **4**(11), 1700337 (2017). https://doi.org/10.1002/advs.201700337

222. M. Benamira, L. Thommy, F. Moser, O. Joubert, M.T. Caldes, New anode materials for it-sofc derived from the electrolyte $BaIn_{0.3}Ti_{0.7}O_{2.85}$ by lanthanum and manganese doping. Solid State Ion. **265**, 38–45 (2014). https://doi.org/10.1016/j.ssi.2014.07.006

223. P.I. Cowin, C.T.G. Petit, R. Lan, J.T.S. Irvine, S. Tao, Recent progress in the development of anode materials for solid oxide fuel cells. Adv. Energ. Mater. **1**(3), 314–332 (2011). https://doi.org/10.1002/aenm.201100108

224. S.Y. Istomin, E.V. Antipov, Cathode materials based on perovskite-like transition metal oxides for intermediate temperature solid oxide fuel cells. Russ. Chem. Rev. **82**(7), 686 (2013). https://doi.org/10.1070/RC2013v082n07ABEH004390

225. D. Chen, C. Chen, Z. Zhang, Z.M. Baiyee, F. Ciucci et al., Compositional engineering of perovskite oxides for highly efficient oxygen reduction reactions. ACS Appl. Mater. Interfaces **7**(16), 8562–8571 (2015). https://doi.org/10.1021/acsami.5b00358

226. Y. Chen, W. Zhou, D. Ding, M. Liu, F. Ciucci et al., Advances in cathode materials for solid oxide fuel cells: complex oxides without alkaline earth metal elements. Adv. Energ. Mater. **5**(18), 1500537 (2015). https://doi.org/10.1002/aenm.201500537

227. Z. Zhang, Y. Zhu, Y. Zhong, W. Zhou, Z. Shao, Anion doping: a new strategy for developing high-performance perovskite-type cathode materials of solid oxide fuel cells. Adv. Energ. Mater. (2017). https://doi.org/10.1002/aenm.201700242

228. Y. Zhu, W. Zhou, Y. Chen, Z. Shao, An aurivillius oxide based cathode with excellent CO_2 tolerance for intermediate-temperature solid oxide fuel cells. Angew. Chem. Int. Ed. **55**(31), 8988–8993 (2016). https://doi.org/10.1002/anie.201604160

229. Z. Shao, Y. Cong, G. Xiong, S. Sheng, W. Yang, Mixed-conducting perovskite-type $Sr_xBi_{1-x}FeO_{3-\delta}$ oxygen-permeating membranes. Sci. China Series B: Chem. **43**(4), 421–427 (2000). https://doi.org/10.1007/BF02969448

230. Z. Shao, G. Xiong, J. Tong, H. Dong, W. Yang, Ba effect in doped $Sr(Co_{0.8}Fe_{0.2})O_{3-\delta}$ on the phase structure and oxygen permeation properties of the dense ceramic membranes. Sep. Purif. Technol. **25**(1), 419–429 (2001). https://doi.org/10.1016/S1383-5866(01)00071-5

231. N. Han, Q. Wei, H. Tian, S. Zhang, Z. Zhu et al., Highly stable dual-phase membrane based on $Ce_{0.9}Gd_{0.1}O_{2-\delta}$-$La_2NiO_{4+\delta}$ for oxygen permeation under pure CO2 atmosphere. Energ. Technol. **7**(5), 1800701 (2019). https://doi.org/10.1002/ente.201800701

232. J. Zhu, G. Liu, Z. Liu, Z. Chu, W. Jin et al., Unprecedented perovskite oxyfluoride membranes with high-efficiency oxygen ion transport paths for low-temperature oxygen permeation. Adv. Mater. **28**(18), 3511–3515 (2016). https://doi.org/10.1002/adma.201505959

233. N. Han, S. Zhang, X. Meng, N. Yang, B. Meng et al., Effect of enhanced oxygen reduction activity on oxygen permeation of $La_{0.6}Sr_{0.4}Co_{0.2}Fe_{0.8}O_{3-\delta}$ membrane decorated by K2NiF4-type oxide. J. Alloy Compd. **654**, 280–289 (2016). https://doi.org/10.1016/j.jallcom.2015.09.086

234. Z. Zhang, Y. Chen, M.O. Tade, Y. Hao, S. Liu et al., Tin-doped perovskite mixed conducting membrane for efficient air separation. J. Mater. Chem. A **2**(25), 9666–9674 (2014). https://doi.org/10.1039/C4TA00926F

235. Z. Zhang, D. Chen, F. Dong, X. Xu, Y. Hao et al., Understanding the doping effect toward the design of CO_2-tolerant perovskite membranes with enhanced oxygen permeability. J. Mem. Sci. **519**, 11–21 (2016). https://doi.org/10.1016/j.memsci.2016.07.043

236. N. Han, Q. Wei, S. Zhang, N. Yang, S. Liu, Rational design via tailoring mo content in $La_2Ni_{1-x}Mo_xO_{4+\delta}$ to improve oxygen permeation properties in CO_2 atmosphere. J. Alloy Compd. **806**, 153–162 (2019). https://doi.org/10.1016/j.jallcom.2019.07.209

237. N. Han, Z. Shen, X. Zhao, R. Chen, V.K. Thakur, Perovskite oxides for oxygen transport: chemistry and material horizons. Sci. Total Environ. **806**, 151213 (2022). https://doi.org/10.1016/j.scitotenv.2021.151213

238. Y. Xu, J. Qu, Y. Li, M. Zhu, Y. Liu et al., Bridging metal-ion induced vertical growth of MoS2 and overall fast electron transfer in (C, P)3N4-M (Ni2+, Co2+)-MoS2 electrocatalyst for efficient hydrogen evolution reaction. Sustain. Mater. Technol. **25**, 00172 (2020). https://doi.org/10.1016/j.susmat.2020.e00172

239. V.R. Stamenkovic, D. Strmcnik, P.P. Lopes, N.M. Markovic, Energy and fuels from electrochemical interfaces. Nat. Mater. **16**(1), 57–69 (2017). https://doi.org/10.1038/nmat4738

240. D. Zhou, X. Xiong, Z. Cai, N. Han, Y. Jia et al., Flame-engraved Nickel-Iron layered double hydroxide nanosheets for boosting oxygen evolution reactivity. Small Methods **2**(7), 1800083 (2018). https://doi.org/10.1002/smtd.201800083

241. J. Tang, X. Xu, T. Tang, Y. Zhong, Z. Shao, Perovskite-based electrocatalysts for cost-effective ultrahigh-current-density water splitting in anion exchange membrane electrolyzer cell. Small Methods **6**(11), 2201099 (2022). https://doi.org/10.1002/smtd.202201099